CALIFORNIA INSTITUTE OF TECHNOLOGY

EARTHQUAKE ENGINEERING RESEARCH LABORATORY

COMPARISON BETWEEN TRANSFER FUNCTION AND MODAL MINIMIZATION METHODS FOR SYSTEM IDENTIFICATION

By

R.T. Beck and J.L. Beck

Report No. EERL 85-06

A Report on Research Conducted Under a Grant
from the National Science Foundation

Pasadena, California
November 1985

CALIFORNIA INSTITUTE OF TECHNOLOGY

EARTHQUAKE ENGINEERING RESEARCH LABORATORY

COMPARISON BETWEEN TRANSFER FUNCTION AND MODAL MINIMIZATION METHODS FOR SYSTEM IDENTIFICATION

by

R. T. Beck and J. L. Beck

Report EERL 85-06

A Report on Research Conducted Under a Grant

From the National Science Foundation

Pasadena, California

November 1985

ACKNOWLEDGEMENTS

R.T.B. would like to acknowledge useful discussions with fellow graduate students L. Paparizos and M. Moser concerning artificial generation of earthquake acceleration signals.

ABSTRACT

The reliability of two methods of structural identification is assessed employing noise-contaminated data.

The statistical properties of the results of the transfer function approach and those of the modal minimization technique are compared, at different levels of noise, with the exact values of the modal parameters being estimated. Comparison indicates that the modal minimization is a far superior technique for structural parameter estimation using linear models.

TABLE OF CONTENTS

1. INTRODUCTION

Models of engineering structures are not complete without the prescription of the values of all parameters involved. For linear models, two techniques, the transfer function approach (TFA) and the modal minimization technique (MMT), provide a means for determining empirical values of these structural parameters directly from the earthquake response of real structures. These values of the parameters can be used to check the accuracy of the values given by methods used in design. They can also be used to provide typical values for parameters, such as damping, which are difficult to determine during the design process.

The most widely applied method is the traditional frequency-domain transfer function approach (TFA) where an attempt is made to estimate modal parameters, mainly the natural frequencies of the lower modes, from properties of the dominant peaks in the transfer function. A number of studies [1,2,3,4,5] have estimated the transfer function from the ratio of the Fourier transforms of the complete time histories of the measured base and response accelerations, although a few have used successive time segments in a moving-window approach to attempt to trace the apparent change in the natural frequencies due to nonlinear behavior [6,7]. These approaches suffer from several difficulties which produce results of questionable reliability. The fundamental difficulty is that estimation of nonparametric models, such as the transfer function, requires long time windows to achieve statistical reliability. Even when the complete acceleration histories are used, the transfer function approach may allow only the

fundamental translational frequencies of a building to be estimated with confidence. The damping estimates are especially questionable. Damping is inherently difficult to estimate accurately with any method, but the problem is accentuated because of the ill-conditioned nature of the calculation of the transfer function from a ratio where the denominator often approaches zero, and because only a few data points are finally used to estimate the damping.

In response to dissatisfaction with the performances of the TFA and other methods for system identification of linear dynamic systems, such as the equation-error method and optimal filter method, output-error techniques were developed to identify linear models from strong-motion records [8,9]. The periods, dampings and effective participation factors of the dominant modes in the reponse are estimated by least-squares minimization of the output-error, which is the difference between either the time histories of the model and recorded responses or their Fourier transforms. The model response is computed using the recorded base accelerations as input. The two methods give effectively the same estimates because of Parseval's identity relating square-integrals in the time and frequency domains. One of the advantages of the output-error methods, of which the MMT is a special case, is that they can substantially reduce the effects of modal interference by simultaneously estimating the parameters of the lower modes. They can also enhance reliability by simultaneously estimating the modal parameters from the measured response at all locations in a building, if more than one location was instrumented. Another advantage is that they can be used to study how well linear models can approximate the strong-motion response of structures since

they provide those values of the parameters of the model which best match the recorded motions. If the match is not satisfactory, then it must be the mathematical form of the model which is at fault and not poor values for the parameters.

Actual results obtained from both the TFA and an output-error method equivalent to the one studied here are presented in Table 1. Estimates for the periods are generally close but those for the damping factors differ substantially. This fact raises the question of the reliability of each method. The purpose of this study is to obtain a better idea about the reliability of the two techniques; in particular, when effects such as noise in the discretized data are taken into account .

The procedure which has been followed in order to study the reliability of the methods is numerical in nature. First, a model is synthesized, i.e., the mechanical model along with all the parameters are defined from the outset so complete knowledge of the properties of the structure is available. Second, the response at some degree of freedom of the structure is calculated numerically using the excitation signal which has been provided together with an appropriate numerical integration scheme. Third, a disturbance is artificially introduced into the input and output signals. In the present study, white noise is superimposed on the respective signals. Fourth, the two techniques are applied to the noise-corrupted signals and the parameters are estimated. Lastly, comparison between the estimates obtained from the techniques and the values used to construct the model provides information about the accuracy and reliability of both techniques.

This procedure is performed on a statistical meaningful test

Building	Direction	T_1(sec) R.3	T_1(sec) R.9	T_2(sec) R.3	T_2(sec) R.9	ξ_1(%) R.3	ξ_1(%) R.9	ξ_2(%) R.3	ξ_2(%) R.9
1900 Avenue of the Stars	N44E	4.27	4.37	1.42	1.45	5.2	4.4	2.0	5.2
	S46E	4.26	4.24	1.41	1.47	6.5	2.2	2.5	5.5
KB Valley Center 15910 Ventura Blvd.	S09W	3.34	3.30	1.17	1.15	11.3	8.6	6.3	8.2
	S18E	3.27	3.05	1.11	1.11	8.9	6.3	6.6	7.6
Sheraton-Universal 3838 Lankershim Ave.	N00W	2.13	1.98	0.66	0.55	4.9	7.3	5.0	8.3
	N90W	2.27	2.24	0.72	0.67	4.1	6.2	8.4	11.6
Bank of California 15250 Ventura Blvd.	N11E	2.38	1.74	0.67	0.49	10.4	12.9	6.0	8.3
	N79W	2.94	1.88	0.98	0.58	9.0	5.8	8.0	5.1
Holiday Inn 8244 Orion Blvd.	N90W	1.26	1.20	0.60	--	16.4	17.3	13.0	--
	N00W	1.49	1.42	0.49	0.30	9.7	19.2	9.2	26.0
Holiday Inn 1640 S. Marengo Ave.	S52W	1.17	1.17	--	--	8.8	5.0	--	--
	N38W	1.03	1.06	--	--	9.0	17.8	--	--

Table 1. Results of two studies [3,9] applying strong-motion identification to records from the 1971 San Fernando earthquake. (After Ref. 10)

sample. The mean of the samples and the standard deviation from the mean value provide a good basis for comparing the results obtained from both techniques.

2. PROCEDURE

The study of the accuracy of the two techniques is performed by a series of numerical tests on synthetic data. An experiment on a real structure presents problems concerning, among others, the large amount of time needed to perform the experiments, the economic resources, and the inaccuracy of the measuring devices. There is also uncertainty in what the correct values of the parameters should be. These and other difficulties can be avoided by using a more analytical approach.

Numerical analyses present the advantage that all the information concerning the structure is well defined since the models of the system and the associated parameters are stipulated from the outset. Numerical errors, such as roundoff, do not present a problem in this study since their magnitudes are much smaller than those of the errors arising from other sources.

2.1. Model of the structure

The structure that was modeled in this study was a ten story building. Since the nature of the excitation was predetermined to be of the form of horizontal ground accelerations, it was acceptable to choose a shear building as the model. The shear building is characterized by columns which offer only lateral flexibility through bending. Viscous damping is assumed to act on the structure in the lateral direction, too. Figure 1 shows the mechanical model for this type of structure.

The stiffness, damping and mass matrices for the structure can be

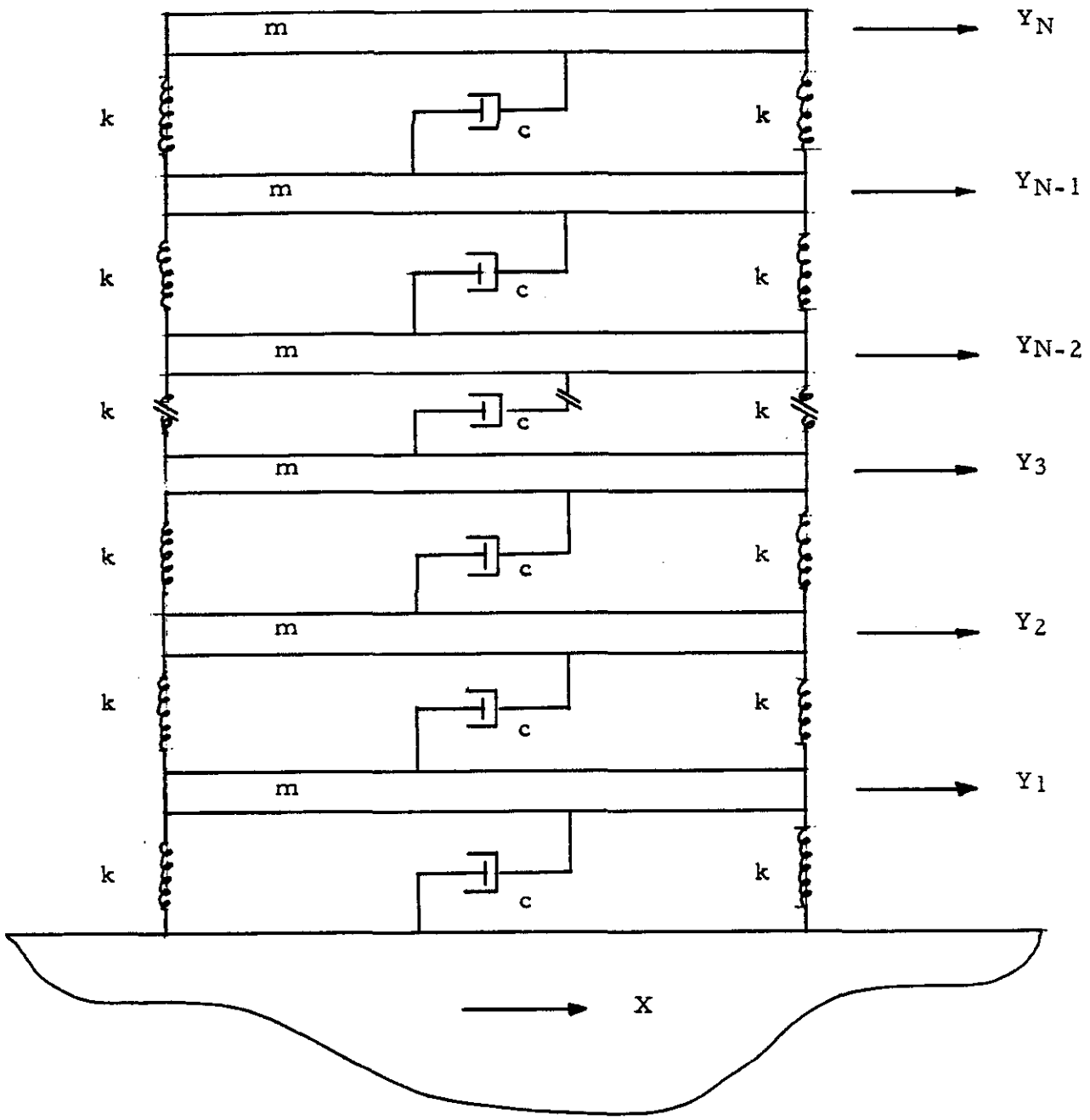

Figure 1 . Damped linear chain model (shear structure) with N degrees of freedom.

easily calculated because of the idealizations mentioned above. The system of equations governing the (lateral) motion of the system can then be written as

$$M\ddot{\underline{Y}} + C\dot{\underline{Y}} + K\underline{Y} = -M\ddot{\underline{X}} \qquad (1)$$

where $\underline{Y}$ is the response vector associated with the degrees of freedom of the structure, M is the mass matrix, C is the damping matrix, K is the stiffness matrix, and $\underline{X}$ is the ground motion. The dots indicate time differentiation. By employing the modal decomposition method the equations are reduced to a system of independent ordinary differential equations [11]. Each differential equation corresponds to a vibrating mode of the structure and takes the form of the governing equation of a single degree of freedom oscillator. The forcing function for each equation is associated with the ground accelerations but not to the solution of the other modal equations, i.e., there is no coupling among the equations.

The parameters of each mode (e.g., natural frequency) are calculated readily given the stiffness, damping and mass matrices. Conversely, given the set of all modal parameters and the mass matrix, it is possible to construct the stiffness and damping matrices [8]. These modal parameters will be taken as the independent set of parameters in the equations. The aim of the study was to determine the values of these parameters using the two techniques and to compare them with the exact values obtained directly from the stiffness, damping and mass matrices. In the following, the set of modal parameters will be denoted by the vector $\underline{a}$:

$$\underline{a} = \{ \omega_i , \xi_i , p_i \; ; \; i = 1, 2, \ldots, N \}$$

Mode #	Natural Period (sec)	Natural (Frequency) (Hz)	Damping Factor	Participation Factor
1	1.0	1.0	0.05	1.2673
2	0.3358	2.978	0.05	-0.4068
3	0.2045	4.890	0.05	0.2259
4	0.1495	6.689	0.05	-0.1429
5	0.1199	8.340	0.05	0.0934
6	0.1019	9.814	0.05	-0.0601
7	0.0904	11.06	0.05	0.0366
8	0.0829	12.06	0.05	-0.0199
9	0.0782	12.79	0.05	0.0087
10	0.0756	13.23	0.05	-0.0021

Table 2. Values of the parameters describing the vibration modes of a ten degree-of-freedom shear building.

where N is the number of modes, and for the i^{th} mode, ω_i is the natural frequency , ξ_i is the damping factor and Pi is the participation factor.

The shear building model consisted of ten floors, i.e., ten degrees of freedom, plus a ground level where the excitation was applied. The exact values of the modal parameters of the structure which are to be estimated are shown in Table 2. These values were computed from expressions given and derived in the appendix.

2.2. Generation of the excitation signal

The excitation of the building model corresponded to that typical of earthquakes, since the aim was to compare these techniques for applications to strong-motion records from structures.

The generation of artificial earthquake acceleration signals has been an active area of research during the last two decades [12]. The approach followed here is simple and yet presents a number of important features characteristic of real earthquake ground acceleration signals.

The steps followed to generate the ground motion signal are shown schematically in Figure 2. The first step of the procedure was to generate a "white-noise" signal, i.e., a discrete signal independently distributed in time with a given Gaussian distribution (zero mean, unit variance) at each time step. This signal was then multiplied by an envelope function which had similar temporal characteristics to those found in real earthquake acceleration signals

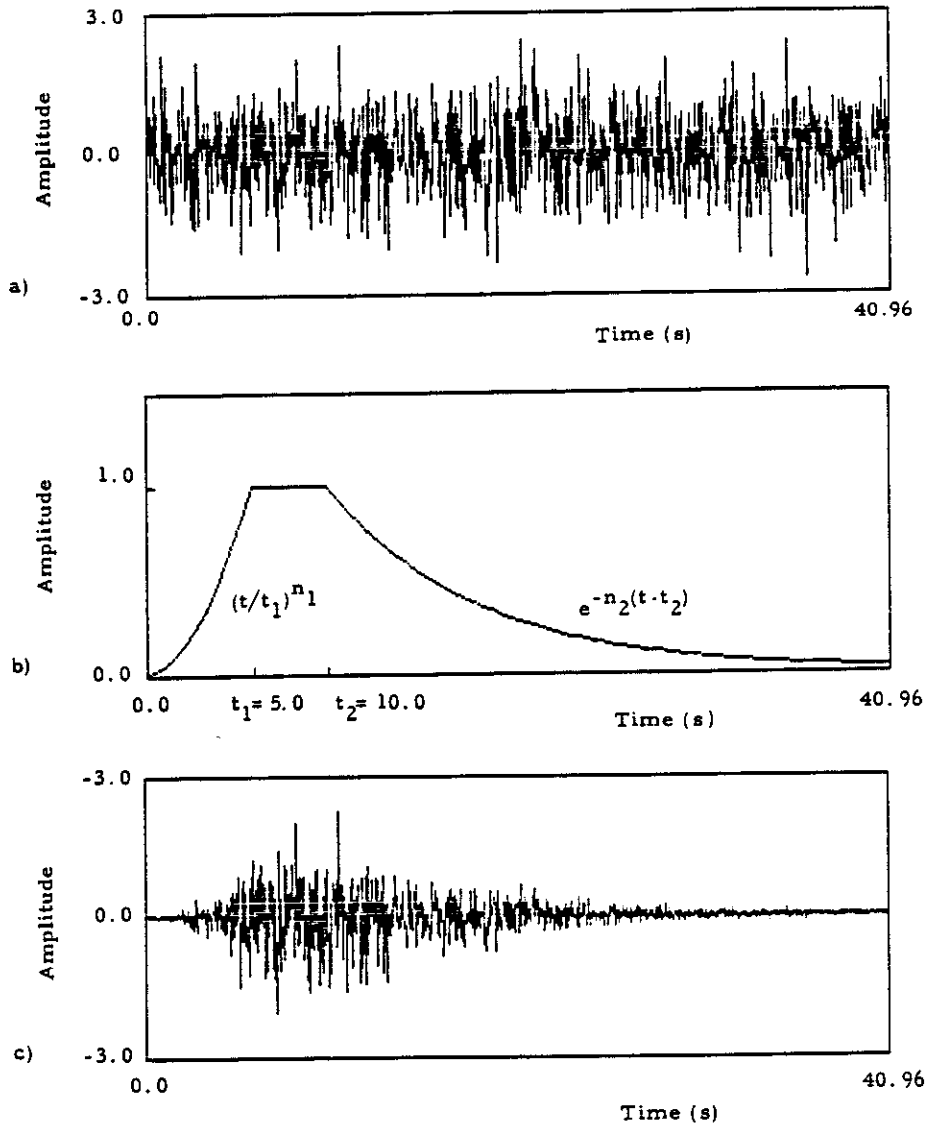

Figure 2. Construction of an earthquake acceleration signal.
a) Gaussian-distributed white noise signal (2048 pts.)
b) Time envelope function (n_1=2, n_2=0.20)
c) Unfiltered signal.

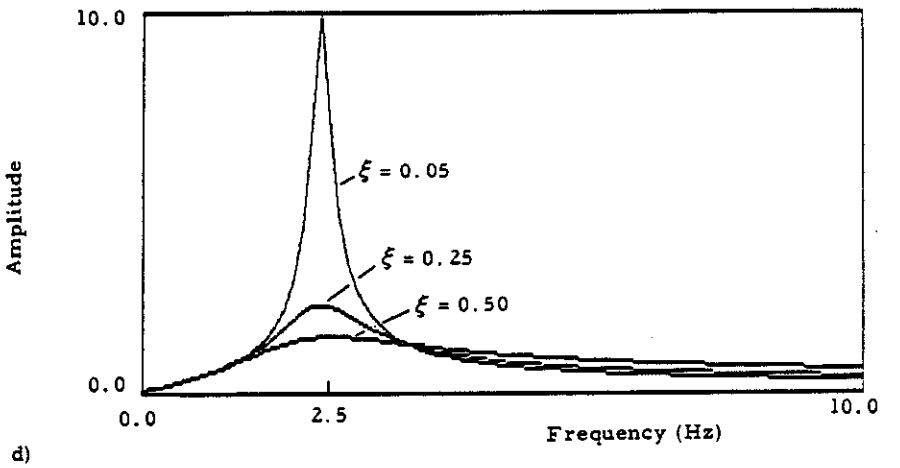

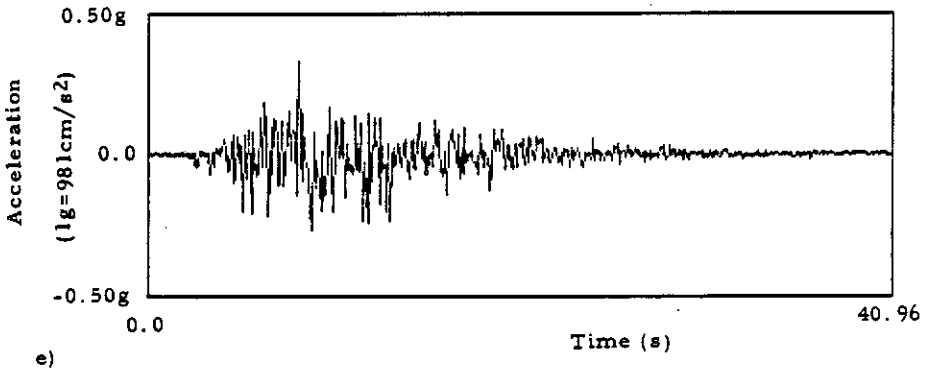

Figure 2, continued.
d) SDOF relative velocity filter (typical ξ=0.50)
e) Final earthquake ground acceleration signal (typical r.m.s. = 50 cm/s^2).

(power-law growth at first, followed by constant magnitude and then exponential decay in the tail). At this point the signal had the correct temporal characteristics but the frequency content was much too uniform. Real earthquake signals present several spectral characteristics, some of which were incorporated in the synthetic signals generated here. For example, near the d.c. level (i.e., 0 Hz) the amplitude rises approximately as the square of the frequency, while at high frequencies the amplitude decays with frequency.

Filtering procedures can be used to modulate the frequency content of an existing signal. The approach followed here corresponded to filtering the signal with a single degree of freedom oscillator. The modulated white-noise signal was treated as the input ground acceleration and the relative velocity of the oscillator was taken to be the output signal. The velocity spectrum takes the correct value of zero at 0 Hz and at high frequencies it decays with frequency. This spectrum, however, does not rise as the square of the frequency near the d.c. level (only the relative acceleration response does). Still, it gives a more realistic frequency content for artificial earthquake signals than that given by the displacement or acceleration of the oscillator. The transfer function of the velocity filter and the resulting signal are shown in Figures 2d and 2e, respectively. Other techniques could have been employed to modulate the frequency spectrum of the signals but the single-degree-of-freedom approach is simple and yet computationally efficient.

The procedure just mentioned was performed on each new signal. In order to lessen any possible bias towards either technique, the parameters governing the time envelope and the single degree of freedom filter were generated with a random routine. The value of the

	Parameter	Mean value	Standard deviation
Time Envelope Function	t_1	3.0 sec	0.5 sec
	t_2	5.0 sec	0.5 sec
	n_1	1.5	0.5
	n_2	0.15	0.05
SDOF	ω	2.5 Hz	0.5 Hz
Filter	ξ	0.70	0.10

Table 3. Typical values of the parameters used to generate earthquake ground motion signals.

parameter in question was always assumed to be Gaussian distributed with a prescribed mean and variance. Typical values of these are shown in Table 3. Figure 3 shows one such earthquake ground acceleration record and its Fourier transform. Comparison with a real acceleration signal is favorable as can be seen in Figure 4.

The noise signals applied to the input and output signals were also constructed as modulated white noise (zero mean, unit variance). Since the tests involved different amounts of noise added to the input and output signals, a measure of the size of the signals was needed. The root-mean-square (r.m.s.) value of the signals was used for this purpose. An r.m.s. value for the the earthquake signal was prescribed and the corresponding value was determined for the response signal. The ratio between the r.m.s. of the noise signal and that for the earthquake or response signals provides an indication of the amount of noise present in the noise-corrupted signals. Various noise-to-signal r.m.s. ratios were employed to study the influence of noise in the reliability of the methods.

Typical signals generated in this study consisted of 2048 acceleration points at a time interval of .02 seconds representing 40.96 seconds of motion. This time interval corresponds to a Nyquist frequency of 25 Hz. Strong motion signals of past earthquakes show very small amplitudes at frequencies over 15 Hz.

2.3. Calculation of the structural response

The response of the system to the excitation signal was calculated using the modal decomposition method. The integration of the equations of motion in the modal domain was performed using the

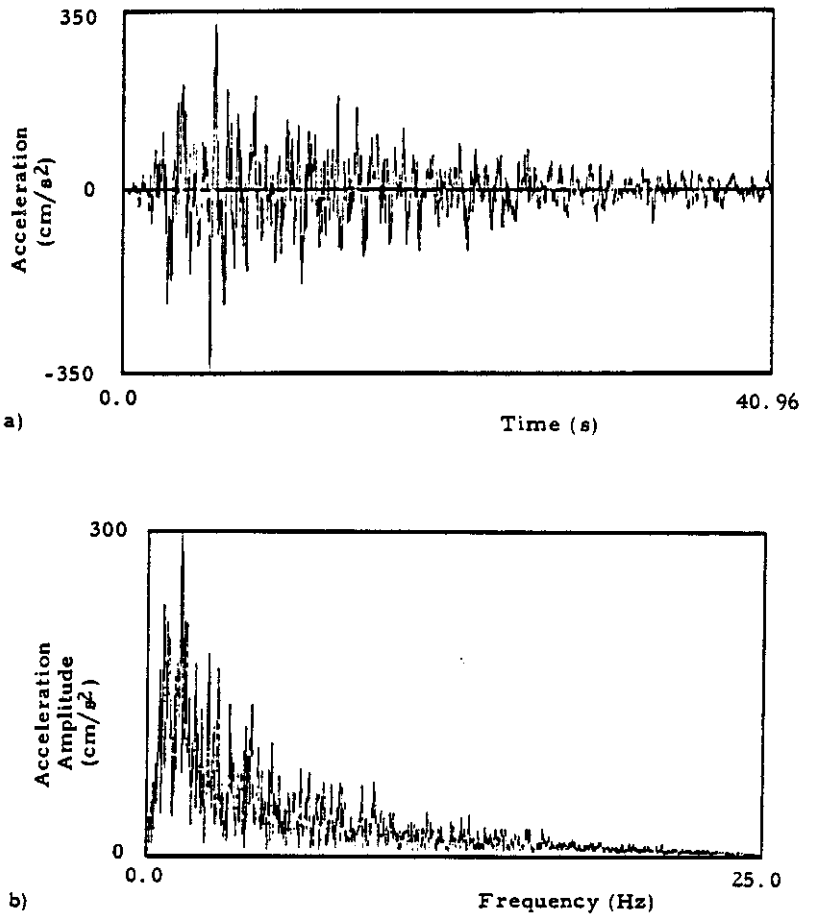

Figure 3. Earthquake ground acceleration signal generated numerically (r.m.s. = 52.42 cm/s^2).
a) Time domain. b) Frequency domain.

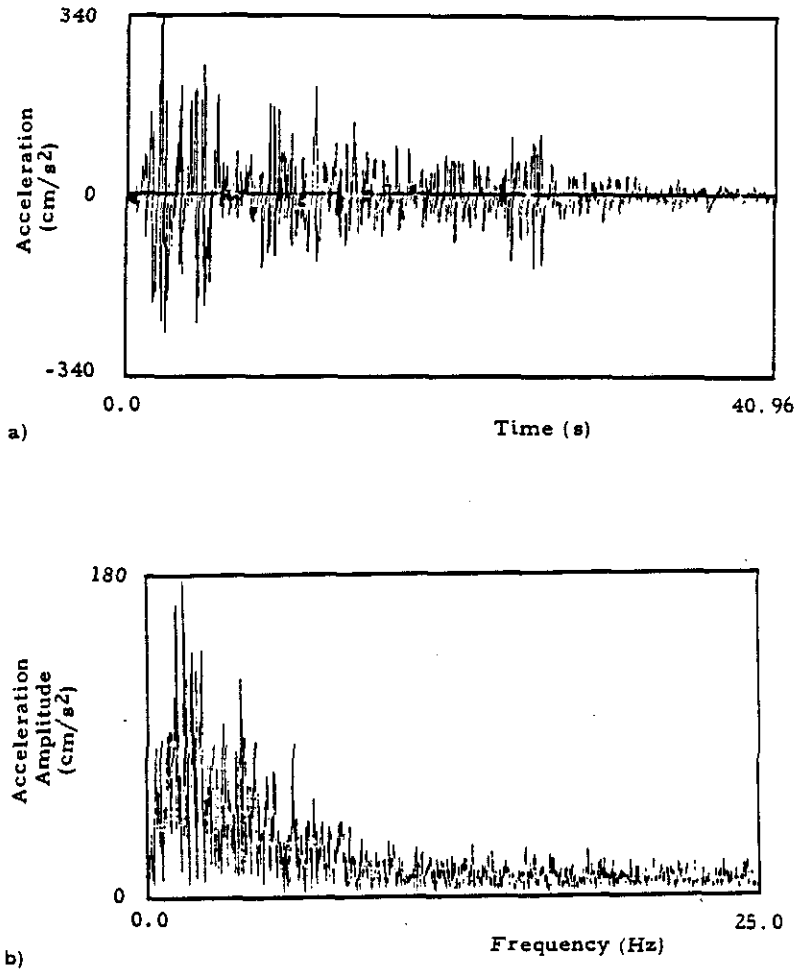

Figure 4. Earthquake ground acceleration signal from El Centro Earthquake 1940 (r.m.s. = 52.41 cm/s^2). a) Time domain. b) Frequency domain.

Nigam-Jennings algorithm [13].

The Nigam-Jennings algorithm is particularly useful for earthquake excitations since it calculates the exact solution to the governing differential equations for each modal single-degree of freedom problem. This solution is exact given that linear interpolation between ground acceleration points is a valid assumption. The motion at any degree of freedom of the structure can then be calculated from the solution of the modal equations and the knowledge of the mode shapes of the structure. Figure 5 presents the response of the tenth degree of freedom (roof response) of the structure to typical earthquake ground acceleration signals (those shown previously in Figures 3 and 4).

2.4. Transfer function technique

The transfer function technique assumes that the structural behavior is linear. This enables the analyst to interpret the structure as a linear filter, i.e., a linear system that modifies the frequency content of the input signal.

The transfer function $H(\omega)$ of the structure (or a filter) is defined by the relation

$$Y(\omega) = H(\omega)\ X(\omega) \qquad (2)$$

where $Y(\omega)$ and $X(\omega)$ are the (complex) Fourier transforms of the recorded roof acceleration and base motion signals of the system, respectively, and ω is the frequency. The initial conditions are assumed to be zero. The amplitude of the complex-valued function $H(\omega)$ will peak close to the natural frequencies if the damping is small.

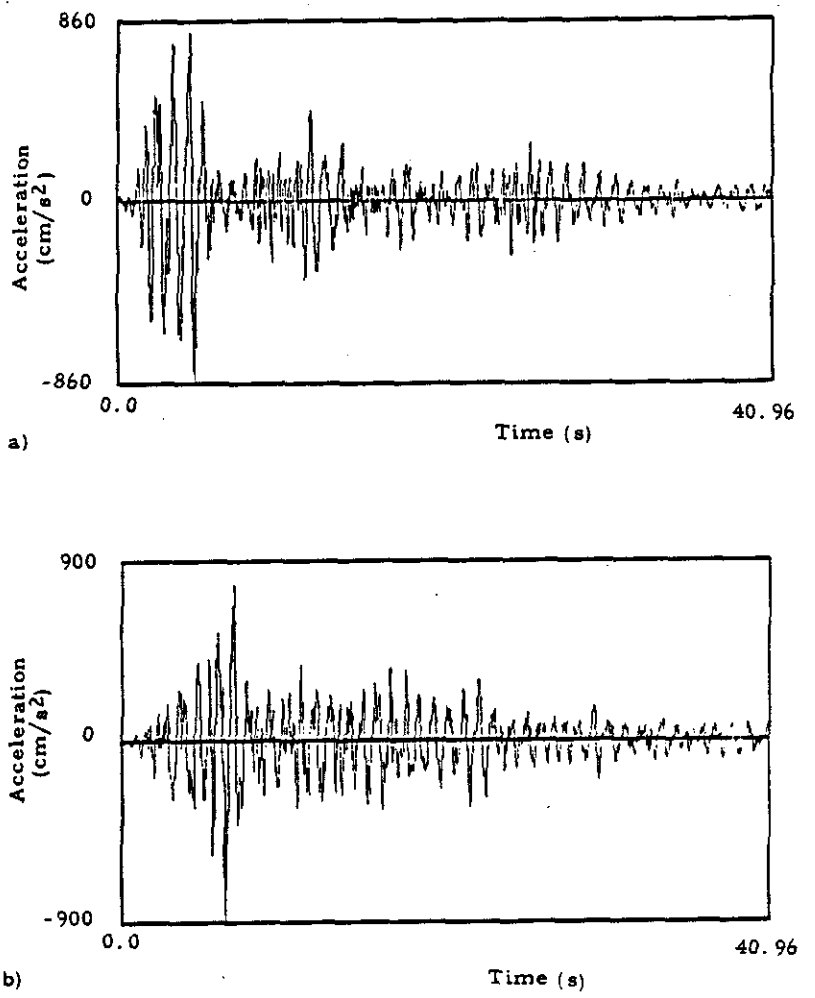

Figure 5. Typical acceleration response of the roof of a ten floor shear building due to a) El Centro earthquake signal, b) numerically generated earthquake signal.

The half-power frequency band-width of the function at the value $\sqrt{2}/2$ of the maximum value is proportional to the amount of damping present in the mode [11]. The height of the amplitude of the transfer function at the natural frequency is proportional to the value of the participation factor for the mode in question.

The absolute value of a typical transfer function for a multiple-degree-of-freedom structure is shown in Figure 6. The inset shows the transfer function for a single-degree-of-freedom oscillator with the corresponding modal parameters. The parameters can be determined from the relative heights and widths of the peak only if the damping is small (narrow peaks). These quantities are more difficult to calculate when there are more than one mode since there is a linear superposition of signals, each coming from a different vibrating mode. If the resonant peaks are narrow enough in order that there is little interference among the modes so that the structural parameters can be determined in a similar way as in the inset of Figure 6, then it is possible to obtain the parameters of interest directly from the plot of $H(\omega)$ versus ω.

Even though the function $H(\omega)$ is complex, only the amplitude of it is useful for determining any structural parameters. The phase information is difficult to utilize since the noise introduces a chaotic-type of phase behavior. Thus the expected phase change of π radians through resonance does not show up clearly. The addition of noise to the input and output signals also causes errors in the empirically determined transfer function. The actual transfer function is given by the relation

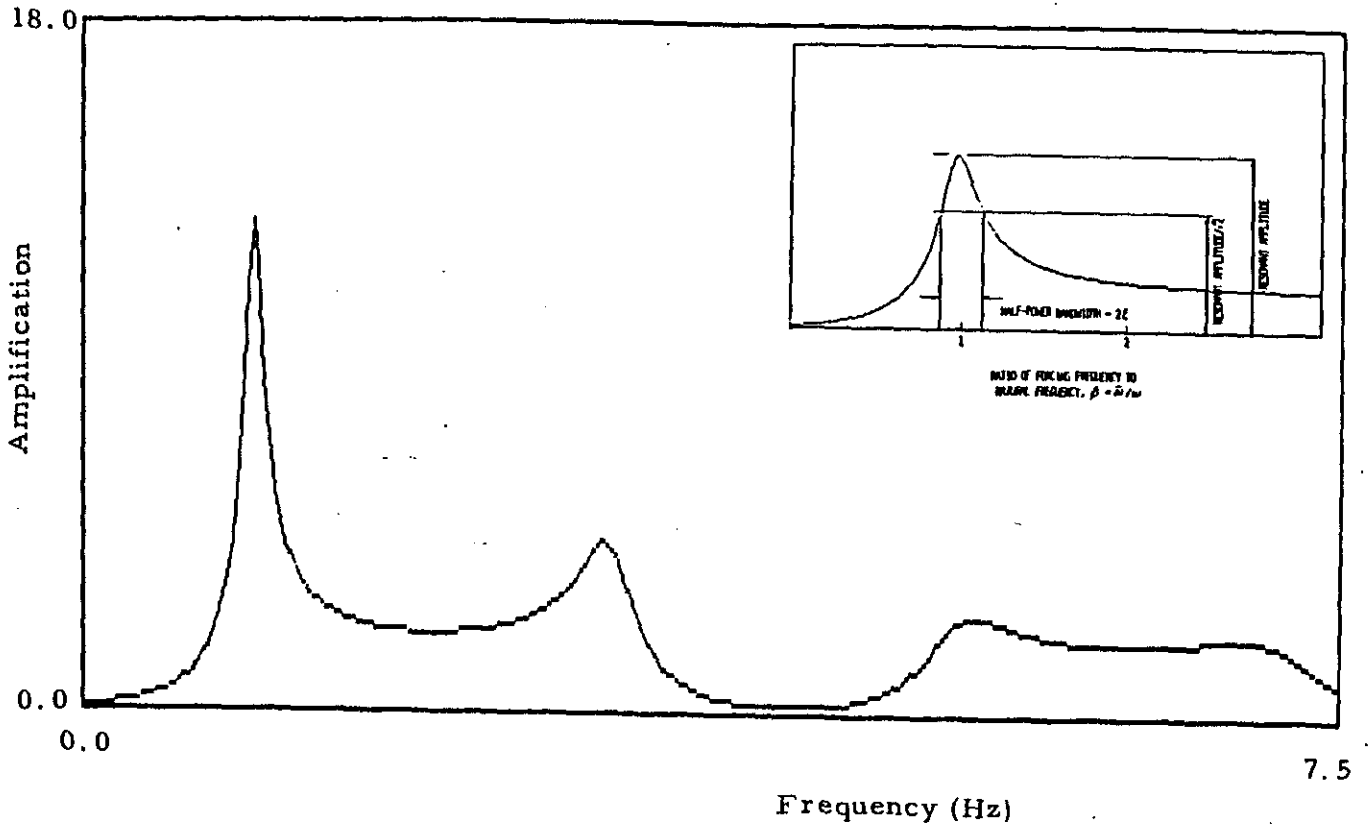

Figure 6. Absolute value of the transfer function of a ten story shear building. Only the peaks corresponding to the first four modes appear in the diagram.

$$H(\omega) = \frac{Y(\omega)}{X(\omega)} \qquad (3)$$

but the empirically determined transfer function $\hat{H}(\omega)$, is given by

$$\hat{H}(\omega) = \frac{Y(\omega) + N_2(\omega)}{X(\omega) + N_1(\omega)} \qquad (4)$$

where $N_1(\omega)$ and $N_2(\omega)$ are the Fourier transforms of two independent noise signals. The amplitude of typical estimated transfer functions corresponding to various noise levels is shown in Figure 7. Comparison between the real transfer functions shown in Figures 8a and 8b, and the ones in Figure 7 indicate that 40 % and 60 % noise levels appear to be representative of real situations (there is the possibility that the "noise" present in the real signals is partly due to modelling errors as well as measurement errors). The procedure followed to estimate the parameters in these high-noise cases involved an operator drawing a curve through the points in such a way that a smooth curve is obtained. It is often possible to distinguish resonant peaks from spurious peaks since noise in long records produces spikes of very narrow widths.

It is important to mention that for the tests done, the operator knew the exact results. Thus, for data containing large noise levels, the results are probably biased in favor of the TFA. If the transfer function of a structure were to be determined from just one record (at noise levels similar to 40%, say, as indicated above), it is probable that poorer estimates would be obtained for the properties of the resonant peaks.

The Fourier transforms were carried out in discrete form using

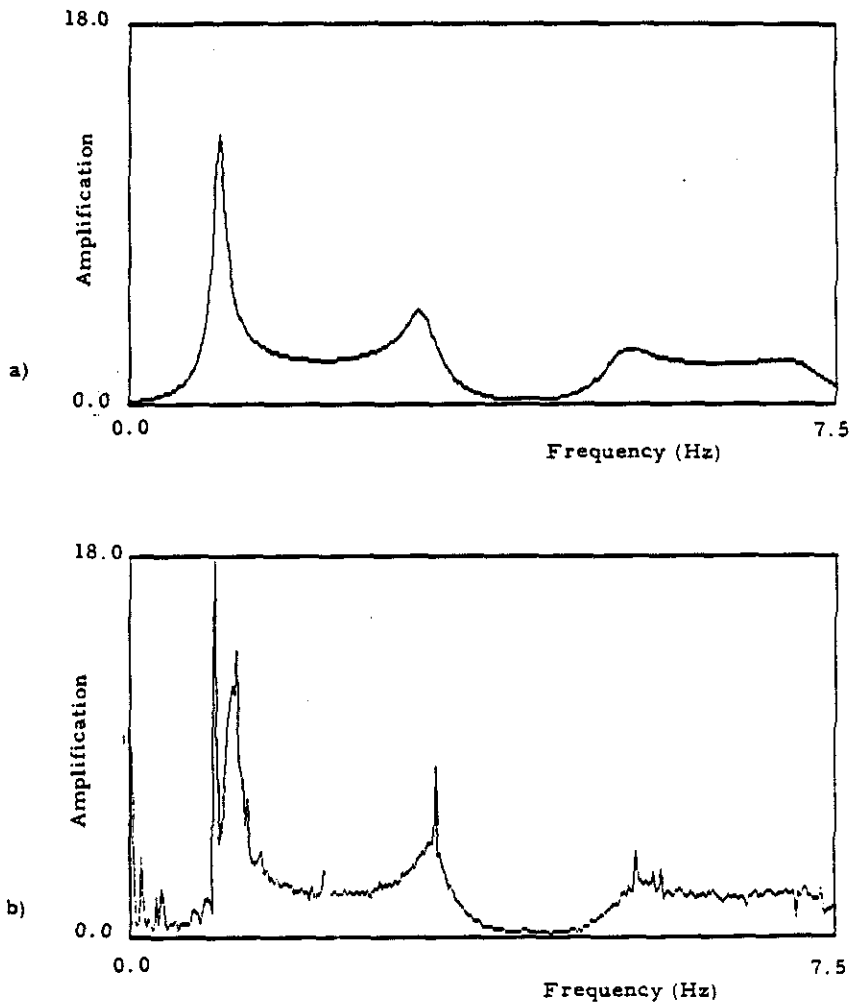

Figure 7. Amplitudes of typical transfer funtions for various levels of noise. a) 0%, b) 20% noise-to-signal contamination added to the input and output of the system.

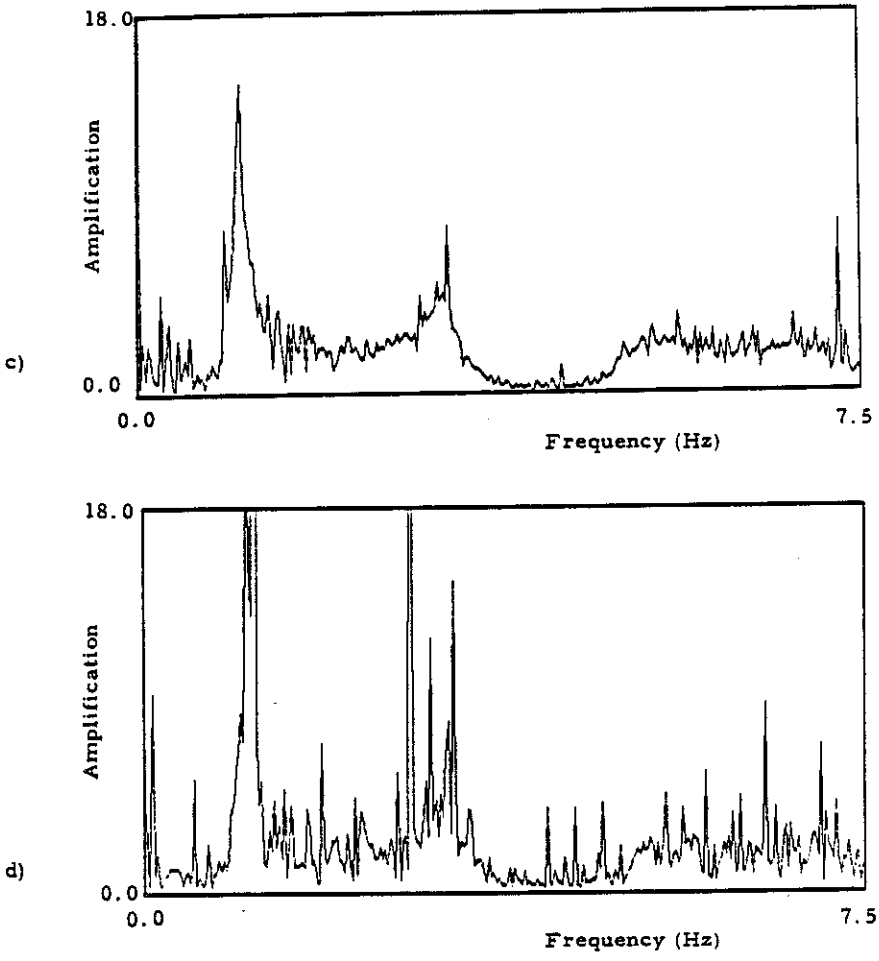

Figure 7, continued.
c) 40%, d) 60% noise-to-signal contamination added to the input and output of the system.

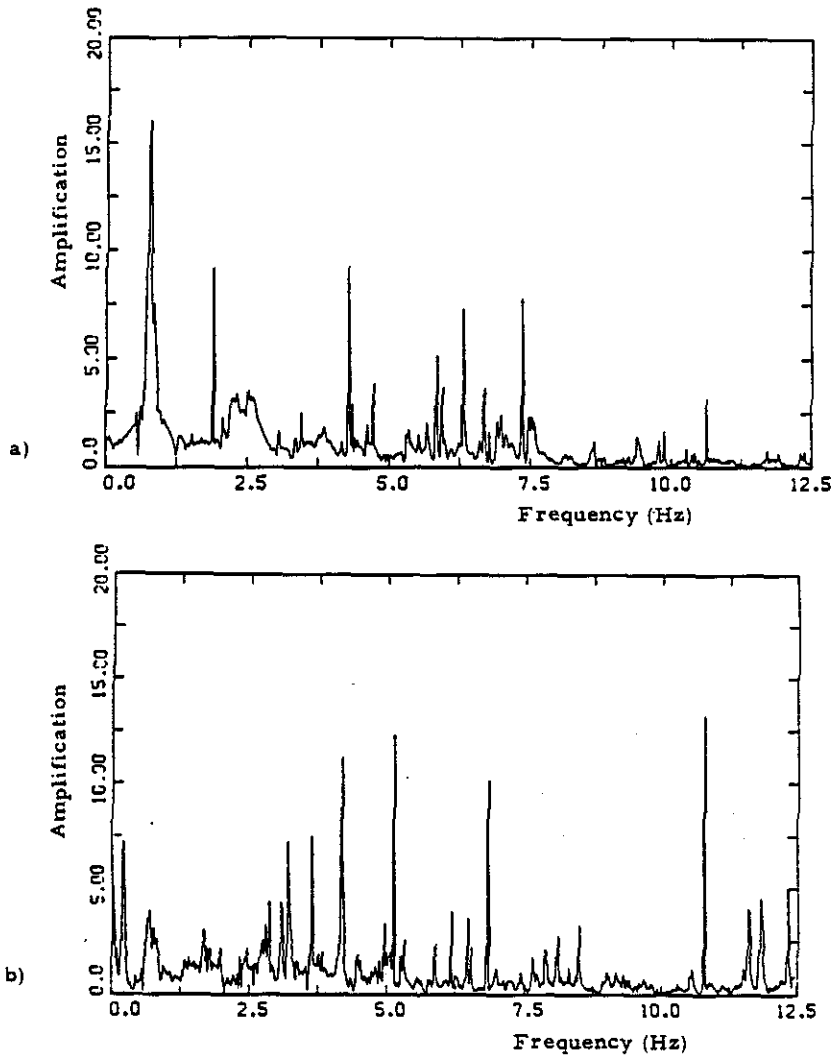

Figure 8. Amplitudes of the empirical transfer functions for two buildings. (Diagrams after Ref. 8)
a) JPL 9-story building 180, Pasadena, CA. Input signal: basement acceleration, output signal: roof response.
b) Union Bank 42-story building, Los Angeles, CA. Input signal: sub-basement acceleration, output signal: 19th floor response.

Hall's FFT algorithm [14]. Typical spectra for the signals ranged from 0 to 25 Hz.

2.5. Modal minimization technique

This technique is based on the concept of minimizing the error between the actual response and the response predicted by the model for a given set of parameters. In an idealized noise-free situation, the minimum error would be zero implying that the actual and predicted responses agreed exactly. In this case, the modal parameters used to obtain the predicted response must be the correct values (see ref. 8 for a discussion of uniqueness of parameter estimates). In practice, however, the minimum error will not be zero because of the presence of noise (inducing errors in the estimates of the modal parameters) or because of model error. The approach requires a useful definition of "error" and an efficient algorithm to vary the values of the parameters in such a way that the minimum value of the error is obtained without excessive computation.

The definition of error used in the automated procedure employed in this study [8] is given by

$$J(\underline{a}) = \int_{t_i}^{t_f} [\, R_a(t) - R_p(t,\underline{X};\underline{a}) \,]^2 \, dt \qquad (5)$$

where $R_a(t)$ and $R_p(t,\underline{X};\underline{a})$ are the actual and predicted responses of the structure in the time interval from t_i to t_f, respectively. The predicted response R_p is computed from the model with modal parameters $\underline{a}$ using the excitation signal $\underline{X}(t)$. The words "response" and "excitation" denote the time history of any of the mechanical

quantities whose observations are available when studying the structure, e.g., accelerations, displacements, stresses, etc. In the present study the response corresponds to the roof acceleration and the excitation to the base acceleration. The integration of the error was performed utilizing Simpson's rule on all discrete data points $R_a(t_n)$ and $R_p(t_n,\underline{X};\underline{a})$ in the time interval from t_i to t_f .

The algorithm employed to vary the parameters in the automated procedure corresponded to a variation of the steepest descent method [8].

3. RESULTS AND DISCUSSION

The results will be shown in the form of graphs of estimated parameter values plotted against noise level. In each graph seven different curves are plotted. The noise-to-signal ratios employed to construct the curves were 0%, 20%, 40% and 60%. Three dashed curves correspond to the results obtained from the modal minimization technique and three dotted curves correspond to the results obtained from the transfer function approach . The solid line corresponds to the exact solution for the parameter under consideration.

For both sets of three curves, the middle curve represents the mean values obtained from a series of ten runs while the two outer curves correspond to the values of the mean plus and minus twice the standard deviation, respectively. In this way an idea of the distribution of the values for each level of noise is obtained. The accuracy of these for the MMT is discussed in section 3.4.

3.1. Periods of oscillation

The periods corresponding to the first three modes were estimated using the two techniques. Figures 9a, b and c present the values for modes 1, 2 and 3, respectively.

A number of features are evident from these graphs. First, the results from both techniques are fairly accurate at all noise levels, the standard deviation growing roughly linearly with noise. It is clear, however, that the MMT is a much more reliable technique for determining the periods of oscillation of the modes. The mean-value

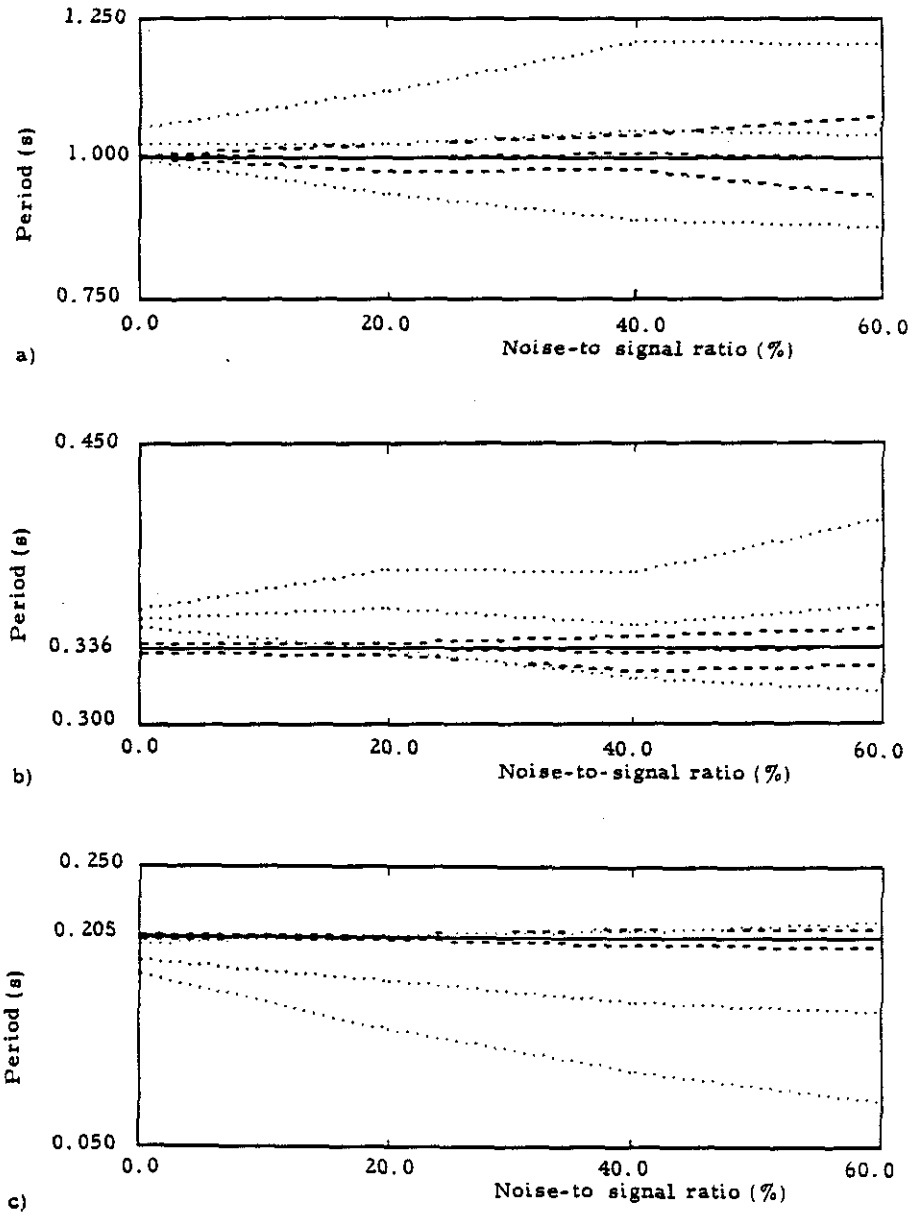

Figure 9. Values of the period of oscillation of the first three modes as estimated by the two techniques plotted against the noise level of the signals. a) First mode, b) second mode and c) third mode.
(Results: ——— exact, ------- MMT, ... TFA)

curves for the MMT results fall close to the exact-value line and the mean-plus-two-standard-deviation curves remain close to the mean-value curve. The results suggest that the larger the mode number, the better the performance of the MMT relative to the TFA.

The mean-value curves for the TFA results are reasonably close to the exact values for the first two modes, but not for the third mode. With no noise, there is a bias in the results for the TFA since the mean-value curves start at a value different from the exact value. One possible reason for this behavior is the fact that the transfer function signals considered were discrete versions of the true transfer function. These discretizations introduced errors since the true peaks in the continuous function were not necessarily identified by the algorithm designed for this purpose. These errors are shown schematically in Figure 10.

There is another possible contribution to this bias. The half-power method assumes that for low levels of damping the natural frequency ω_n differs negligibly from the frequency ω_p at which the transfer function peaks. Analytically, this is written as

$$\omega_n \cong \omega_p = \frac{\omega_n}{\sqrt{1 - 2\xi^2}}$$

At 5 % damping, say, ω_p is approximately 1.0025 ω_n which implies that the natural frequency ω_n differs by 0.25 % , approximately, from the "peak" frequency ω_p . The bias in the graphs show that ω_n , as calculated by the TFA, is in error by -0.9%, -1.9% and 2.3 % in modes 1, 2 and 3, respectively. Thus it is possible that this approximation contributed significantly to the error, particularly for the first mode results.

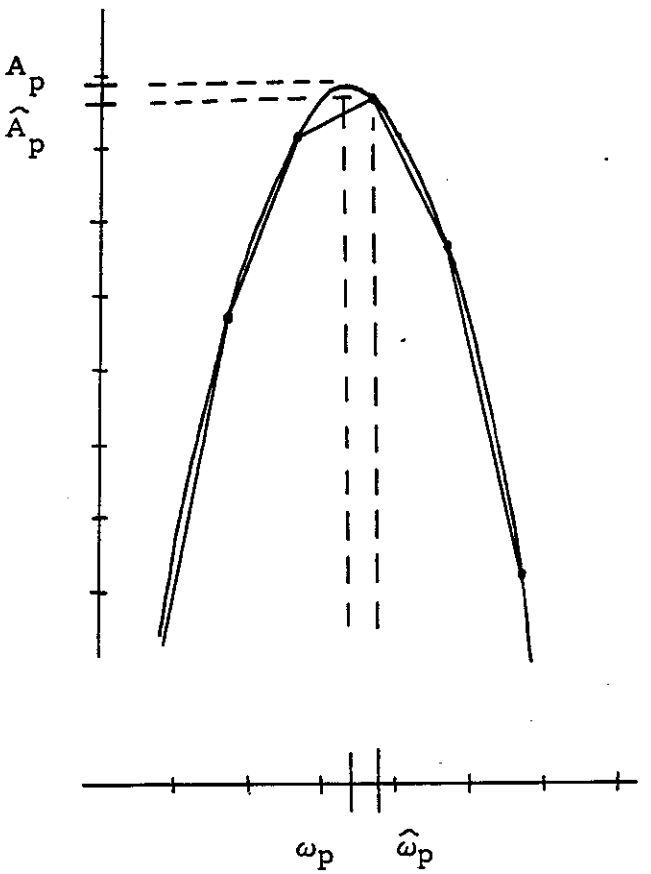

Figure 10. Introduction of errors into the TFA results from the discretization procedure. $\hat{A}_p$ and $\hat{\omega}_p$ are the approximate resonant amplitude and frequency. A_p and ω_p are the exact values.

Bias in the results of the MMT, if any, may be due to the fact that the algorithm is an iterative one and the solution may not have converged to the exact value. Improvement can be guaranteed if a smaller tolerance level of convergence is assigned. Computational time, however, may increase dramatically if the convergence levels are reduced to the same order as the numerical roundoff error.

3.2. Damping factors

Figures 11a, b and c show the curves for the variations of the values of the damping factors with noise level.

Again, the results show that the MMT gives much more reliable estimates than the TFA. Also, the results from the TFA show erratic behavior. The mean-value curves do not seem to follow any consistent pattern and their values are far off from the exact value. This is more pronounced at larger values of noise, as expected. There is a bias at the zero noise level as for the periods. This may be due to the fact that the peaks were not calculated accurately and when calculating $\sqrt{2}/2$ of the peak amplitude, a level too low on the resonant peak is obtained. This then means that the half-power bandwidth is too large when determining the damping factor. Besides this source of error, there is also interaction among the modes. The peaks of the transfer function can be skewed to either side depending on where the interacting mode is located in the frequency domain relative to the natural frequency being considered. This is also a reason for bias in the periods. Figure 12 shows schematically this influence.

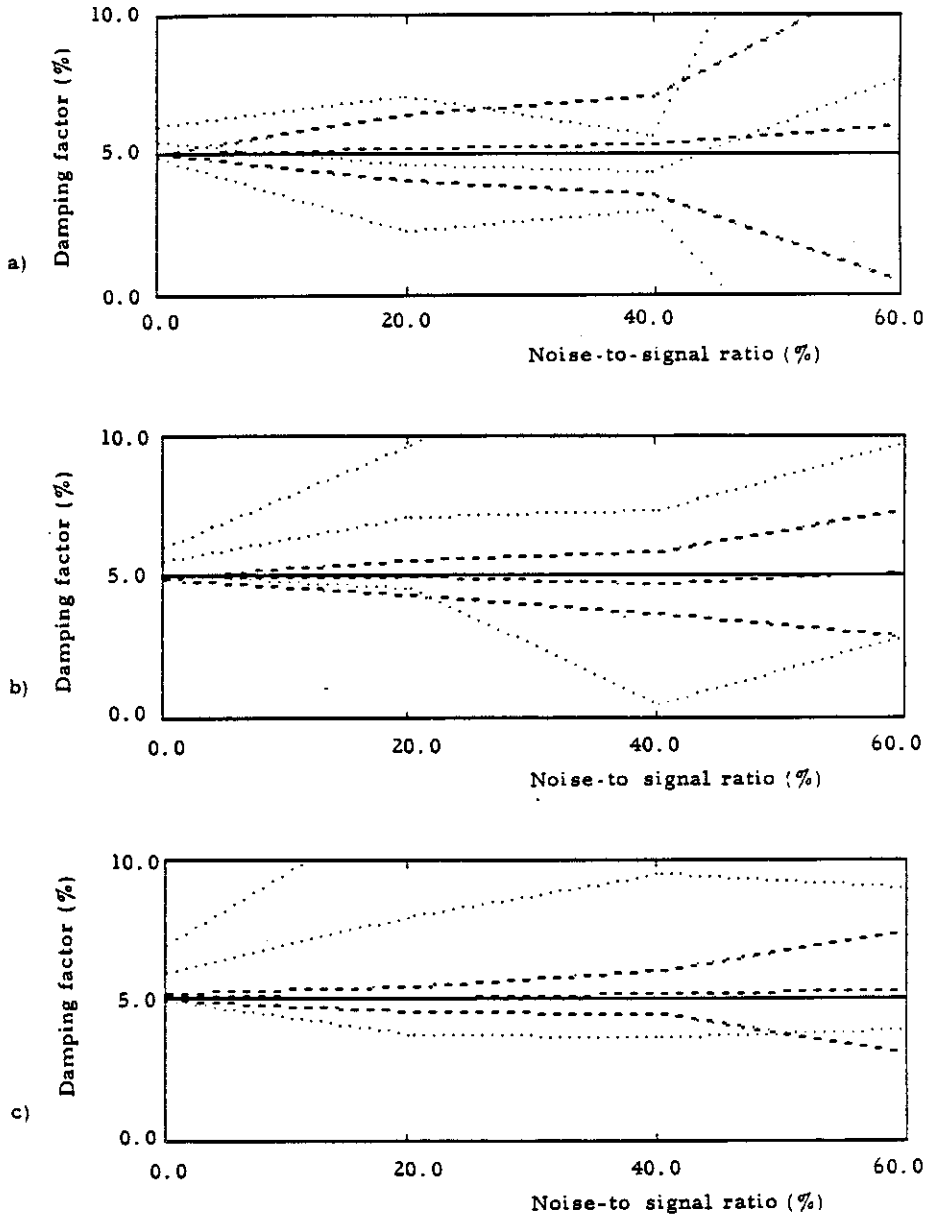

Figure 11. Values of the damping factor of the first three modes as estimated by the two techniques plotted against the noise level of the signals. a) First mode, b) second mode and c) third mode.
(Results: ——— exact, - - - - - - MMT, ... TFA)

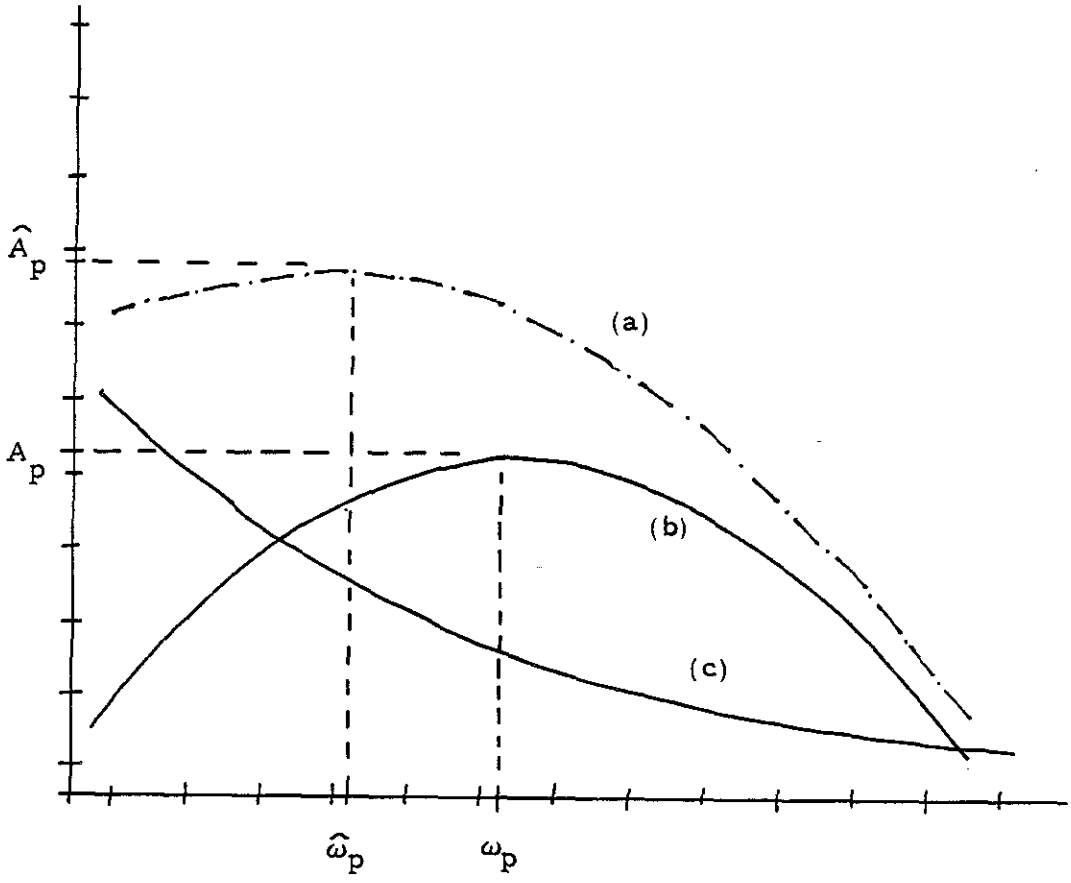

Figure 12. Modal interference produces bias in the estimates of the resonant frequencies and amplitudes. Curve (a) is the sum of the modal curve (b) in question plus the decaying curve (c) of the interfering mode, including the effects of phase. $\hat{A}_p$ and $\hat{\omega}_p$ are the approximate resonant amplitude and frequency. A_p and ω_p are the exact values.

The mean-plus-two-standard-deviations curves for the TFA show erratic behavior, too. The standard deviation values should only be used as an indication of the scatter of the results. In Figure 11a the curves for the fundamental mode seem to indicate the existence of negative values of the damping factor in the noise level region above 40 %, but the numerical results (and physical requirements) constrain the values to be in the positive range. Actually, this implies that the distribution of the values cannot be taken to be Gaussian. Due to the lack of information of the type of distribution and to the lack of a large sample of data, care must be taken in interpreting the mean-plus-two-standard-deviations curves when their values are well away from the mean value.

The results of the TFA exhibit another characteristic which was not expected. The standard deviation values decreased at some higher noise levels in the signals. This feature can be seen in the narrowing of the "standard deviation" curves (see, for example, noise levels 20 and 40 % for mode 1, noise levels 40 and 60 % for mode 3). One possibility that explains this behavior is that the operator is able to discern noise when the latter presents itself as narrow peaks, but the results may be biased when noise appears in other forms. This implies that the number of samples is not large enough to obtain a statistically significant distribution for the TFA values at each noise level (even though the number of samples was large enough for the MMT, which gives much smaller standard deviations).

The results from the MMT are more consistent than those from the TFA in that the mean-value curve does not show large discrepancies with respect to the exact-value line. The "standard deviation" curves also show more consistent behavior: the separation of the curves

increases proportionately to the noise level. What is not fully understood is the fact that the reliability of the results improves as the mode number is increased. Normally, this would not be expected since the higher the mode, the poorer the signal-to-noise level.

3.3. Participation factors

The values obtained for the roof participation factors are shown in Figures 13a, b and c.

The curves from the TFA are, again, somewhat erratic, especially in the second and third modes. The mean-value curve in all graphs is biased away from the exact-value line. The trend is more visible as the mode number increases. The "standard deviation" curves spread out considerably as the noise level increases, except for the third mode from the 40% to the 60 % noise level, where the standard deviation curves contract. The results show that the TFA is very unreliable since the scatter is large and, in modes 2 and 3, the exact-value line falls outside the region bounded by the "standard deviation" curves.

The results from the MMT are more reliable than those from the TFA but still do not predict the values accurately. In mode 1 the mean-value curve veers away from the exact-value line and the mean-plus-two-standard-deviations curve indicates that the scatter is small, so the results will consistently predict values smaller in magnitude than the exact. The results for modes 2 and 3 also indicate a bias in the MMT results, but it is smaller than for mode 1. The bias in the results can be introduced since the error functional $J(\underline{a})$ is sensitive to the ratio of the damping factor to the participation

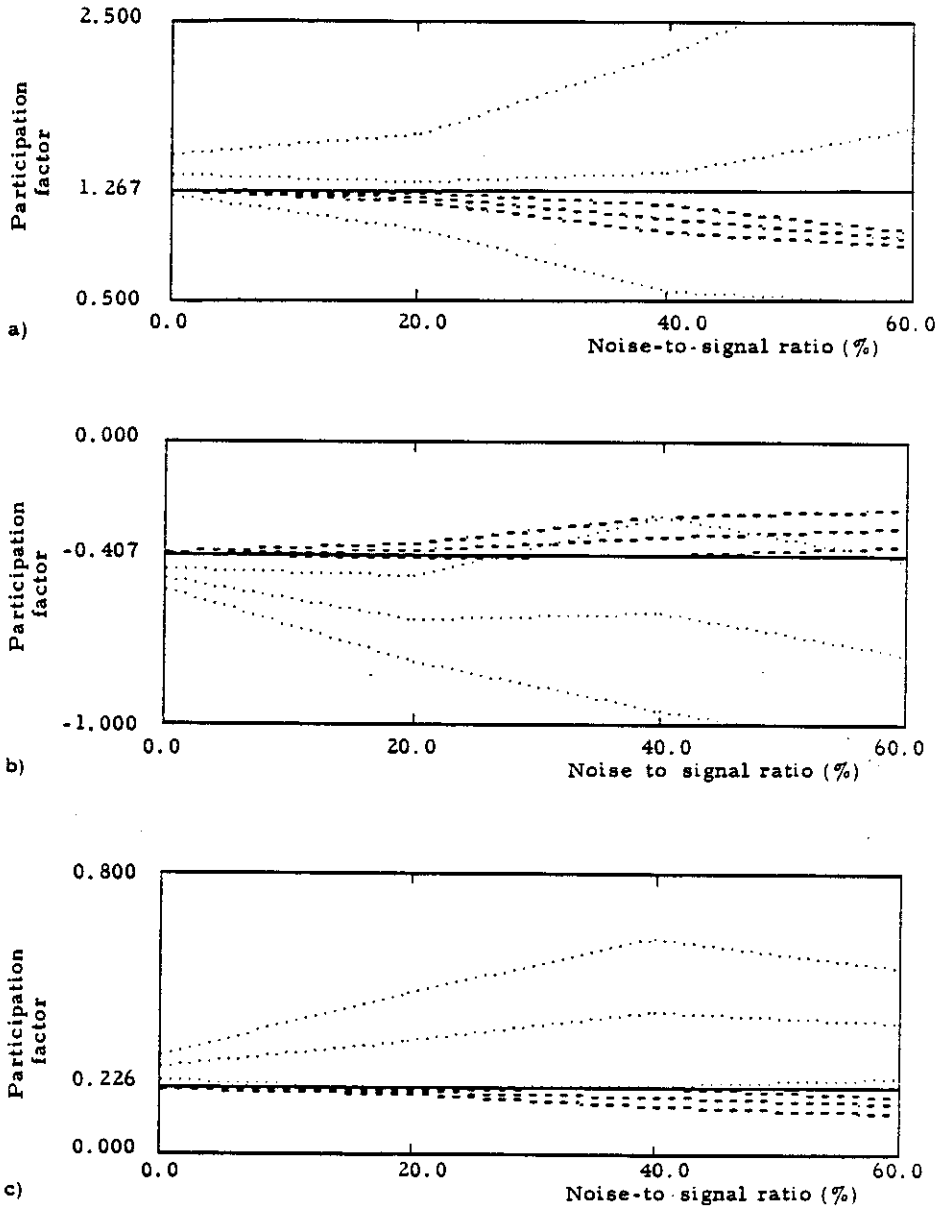

Figure 13. Values of the participation factors of the first three modes as estimated by the two techniques plotted against the noise level of the signals. a) First mode, b) second mode and c) third mode.
(Results: ——— exact, ------- MMT, ····· TFA)

factor but not to their independent values [8].

3.4 Statistical validity of the MMT results

The statistical validity of the MMT results was evaluated by comparing the results obtained from samples with increasing sizes. The values of the modal parameters for the ten story shear building were estimated for the following sample sizes: 2, 5, 10, 15, 20, 25, 30, 40, 50, 60, 80 and 100. The input and output record signals were corrupted with a fixed 20% noise-level (i.e., 20% noise-to-signal r.m.s. ratio).

The variation of the statistical parameters with sample size are shown in Figures 14a, b and c. In these figures, three solid lines are drawn and correspond to the mean and the mean plus and minus twice the standard deviation, respectively. Comparison between the values for a sample-size of ten with those belonging to larger sample sizes indicates that the results shown in previous sections are statistically meaningful.

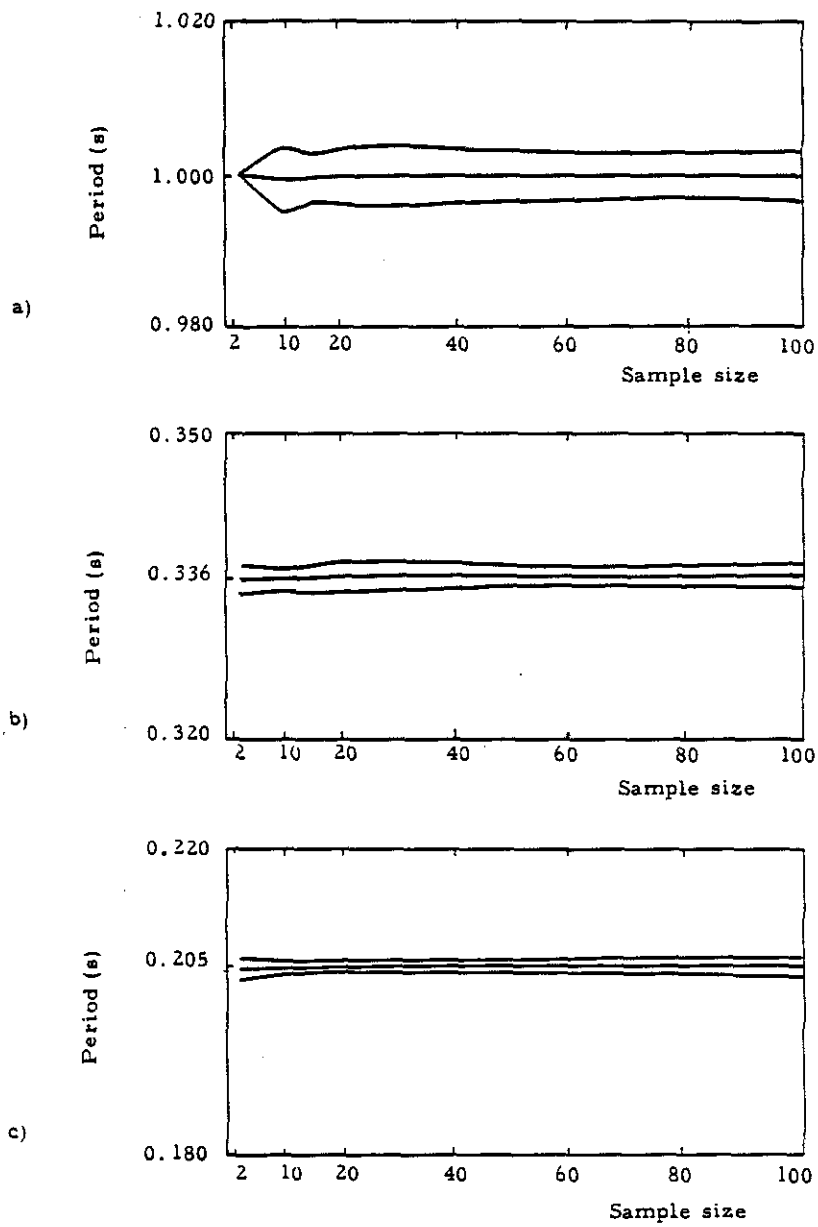

Figure 14. Values of the period of oscillation for the first three modes of a ten degree-of-freedom shear building plotted at various sample sizes. The parameter estimates were obtained from a 20% noise level corrupted signal. a) First mode, b) second mode and c) third mode.

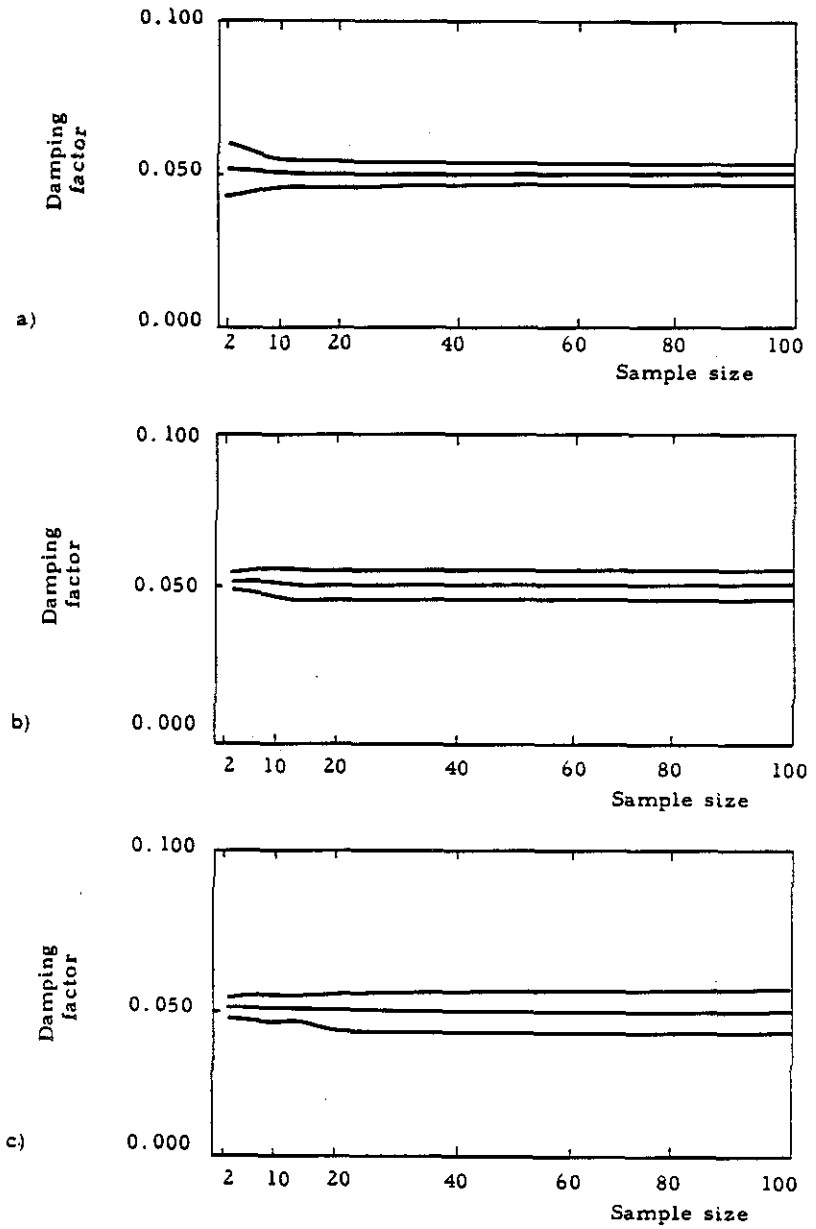

Figure 15. Values of the damping factor for the first three modes of vibration of a ten degree-of-freedom shear building plotted at various sample sizes. The parameter estimates were obtained from a 20% noise level corrupted signal. a) First mode, b) second mode and c) third mode.

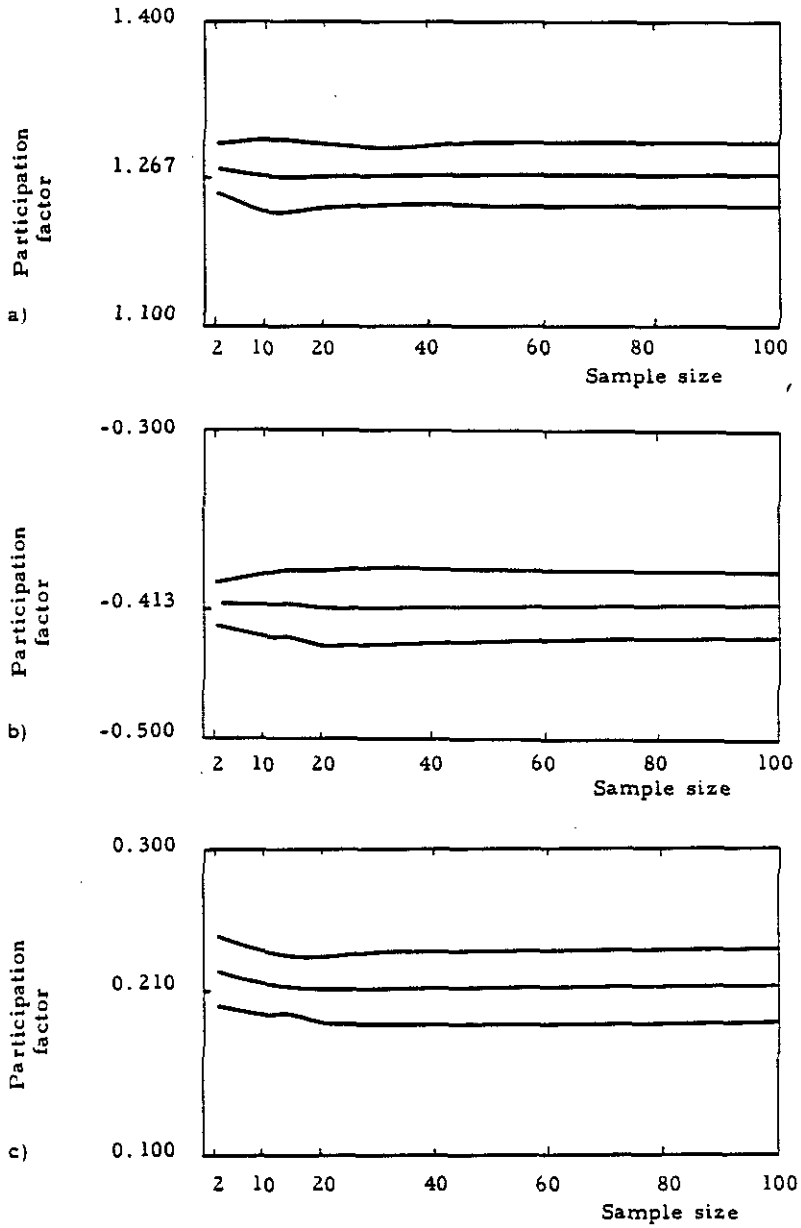

Figure 16. Values of the participation factor for the first three modes of vibration of a ten degree-of-freedom shear building plotted at various sample sizes. The parameter estimates were obtained from a 20% noise level corrupted signal. a) First mode, b) second mode and c) third mode.

4. CONCLUSIONS

The comparison of the numerical results for a sample of ten tests show that the MMT (modal minimization technique) is a much more accurate and reliable technique than the TFA (transfer function approach) for estimating the values of the periods, damping factors and participation factors of the first few modes of vibration of an engineering structure. In these tests, the periods were estimated most accurately while the damping and participation factors showed larger scatter.

The better performance of the MMT can be attributed to a number of factors. First, the MMT makes use of all the information in the data whereas the TFA concentrates on data in the neighborhood of peak and half-power points. Second, the reliability of the TFA is worsened because of the discrete nature of the computed transfer function. Third, the TFA becomes unreliable when modal interference is strong while the MMT is relatively insensitive to it. Finally, the MMT imposes a parametric model from the outset whereas the TFA imposes it only after the empirical transfer function has been determined, so there are more physical contraints in extracting the model from the noise-contaminated data in the MMT.

REFERENCES

1. G. C. Hart, "1901 Avenue of the Stars Building" in San Fernando, California, Earthquake of February 9, 1971, 1, U.S. Dept. of Commerce, Washington, D.C. 1973.

2. J. H. Wood, "Analysis of the Earthquake Response of a Nine-story Steel Frame Building during the San Fernando Earthquake", Rep. EERL 72-04, Caltech, Pasadena, Ca. 1972.

3. G. C. Hart and R. Vasudevan, "Earthquake Design of Buildings: Damping", J. Struct. Div., ASCE, 101, ST1, pp. 11-29. 1975.

4. G. C. Hart, R. M. DiJulio, and M. Lew, "Torsional Response of High-rise Buildings", J. Struc. Div., ASCE, 101, ST1, pp. 397-416. 1975.

5. A. M. Abdel-Ghaffar, "Engineering Data and Analyses of the Whittier, California, Earthquake of January 1, 1976", Rep. EERL 77-05, Caltech, Pasadena, Ca. 1977.

6. F. E. Udwadia and M. D. Trifunac, "Time and Amplitude Dependent Response of Structures", Earthq. Eng. Struc. Dyn., 3, pp. 183-201. 1974.

7. J. M. Pauschke, C. S. Oliveira, H. C. Shah, and T. C. Zsutty, "A Preliminary Investigation of the Dynamic Response of the Imperial County Services Building during the October 15, 1979 Imperial Valley Earthquake", Rep. 49, Dept. of Civil Eng., Stanford University, Stanford, Ca. 1981.

8. J. L. Beck, "Determining Models of Structures from Earthquake Records", Rep. EERL 78-01, Caltech, Pasadena, Ca. 1978.

9. G. H. McVerry, "Frequency Domain Identification of Structural Models from Earthquake Records", Rep. EERL 79-02, Caltech, Pasadena, Ca. 1979.

10. J. L. Beck, "System Identification Applied to Strong Motion Records from Structures", in Earthquake Ground Motion and its Effects on Structures, AMD, 53, ASME, pp. 109-133. 1983.

11. R. W. Clough and J. Penzien, Dynamics of Structures, McGraw Hill, New York, N. Y. 1975.

12. R. E. Scholl and J. L. King (eds.), Strong Ground Motion Simulation and Earthquake Engineering Applications. A Technological Assessment, EERI, Berkeley, Ca. 1985.

13. N. C. Nigam and P. C. Jennings, "Calculation of Response Spectra from Strong-motion Earthquake Records", Bull. Seismo. Soc. America, 59, 2, pp. 909-922. 1969.

14. J. F. Hall, "An FFT Algorithm for Structural Dynamics", Earthq. Eng. Struc. Dyn., 10, pp. 797-811. 1982.

APPENDIX A

DERIVATION OF THE MODAL PARAMETERS OF A SHEAR BUILDING MODEL

The equations of motion are given by equation (1), i.e.,

$$M\ddot{\underline{Y}} + C\dot{\underline{Y}} + K\underline{Y} = -M\ddot{\underline{X}} \quad . \qquad (A1)$$

Because of the nature of the relative motion $\underline{Y}$, the base acceleration $\ddot{\underline{X}}$ can be written as $\ddot{X}\underline{i}$ where $\underline{i}$ is the vector with N components

$$\underline{i} = \{ 1, 1, 1, \ldots, 1 \} . \qquad (A2)$$

Due to the properties of the shear building models, the matrices M, C and K take the following forms:

$$\begin{aligned} M &= m\,I \\ C &= c\,U \\ K &= k\,U \end{aligned} \qquad (A3)$$

where I is the identity matrix and U is a symmetric matrix of the form

$$U = \begin{bmatrix} 2 & 1 & 0 & 0 & \ldots & & \\ 1 & 2 & 1 & 0 & 0 & \ldots & \\ 0 & 1 & 2 & 1 & 0 & 0 & \ldots \\ 0 & 0 & 1 & 2 & 1 & 0 & 0 \quad \ldots \\ \ldots & & & & & & \end{bmatrix}$$

The values m, c and k are defined schematically in Figure 1. This matrix U can be decomposed into $U = 2\,I + W$, where W is the matrix of off-diagonal ones shown in the matrix above.

A1. Eigenfrequencies and eigenvectors

The eigenfrequencies and eigenvectors are found by considering the homogeneous problem

$$M \ddot{\underline{Y}} + K \underline{Y} = \underline{0} . \qquad (A4)$$

The damping matrix would have normally changed the eigensolution but for shear buildings the modeshapes for the damped and undamped problems are identical since the damping matrix C satisfies the equation $C M^{-1} K = K M^{-1} C$, [A-1].

A form of the solution $\underline{Y} = \underline{f} \sin(\omega t+\theta)$ is introduced into Equation A4. In the last expression, $\underline{f}$ is the modeshape, ω is the frequency, t is time and θ is the phase. Equation A4 then becomes

$$-\omega^2 M \underline{f} + K \underline{f} = \underline{0} \qquad (A5)$$

and after substituting in for M and K

$$U \underline{f} = \mu \underline{f} \qquad (A6)$$

where $\mu = \omega^2 (m/k) > 0$, since M and K are positive definite. After introducing the expression for U in Equation A6, the following expression is obtained

$$W \underline{f} = (2 - \mu) \underline{f} = \lambda \underline{f} . \qquad (A7)$$

From Equation A7 the following difference equation is obtained:

$$f_{i-1} + f_{i+1} = \lambda f_i \qquad i \in \{ 1, 2, \ldots, N \} \qquad (A8)$$

It is required that $f_0 = 0$ and $f_{N+1} = f_N$. Assuming a form for $\underline{f}$, such as

$$f_i = \sin(ai) , \qquad (A9)$$

and after introducing it into Equation A8, leads to the relation

$$\begin{aligned} \lambda \sin(ai) &= \sin[a(i-1)] + \sin[a(i+1)] \\ &= 2 \sin(ai) \cos(a) . \end{aligned} \qquad (A10)$$

It must be the case that $\lambda = 2 \cos(a)$. Also, since $f_{N+1} = f_N$,

$$\sin[a(N+1)] = \sin(aN)$$

This implies that 'a' must satisfy the relation

$$a(N+1) = (-1)^j aN + j\pi \qquad j \in \{1, 2, \ldots\}$$

or, equivalently,

$$a = \frac{j\pi}{1 + N[1-(-1)^j]} . \qquad (A11)$$

If j is even then $\sin(ai) = 0$ and thus $\underline{f} = \underline{0}$. If j is odd then the expression above simplifies to

$$a_j = \frac{j\pi}{2N+1} . \qquad (A12)$$

The final expression for λ is

$$\lambda = 2 \cos\left(\frac{2j-1}{2N+1}\pi\right) \qquad (A13)$$

and that for ω_j is

$$\omega_j = 2\sqrt{k/m}\ \sin\left(\frac{2j-1}{2N+1}\,\frac{\pi}{2}\right) . \qquad (A14)$$

It is clear that given the values for k and m, it is possible to generate the frequencies for all modes. For the tests performed in this study, the value of ω_1 was arbitrarily set to 2π rad s^{-1}. This defines the value for the ratio $\sqrt{k/m}$ and so the values of all other frequencies are readily computed as shown in Table 2. The eigenvectors corresponding to these eigenfrequencies are given by

$$f_i^{(j)} = \sin(a_j i) = \sin\left(\frac{2j-1}{2N+1}\, i\pi\right) \qquad (A15)$$

where i represents the degree-of-freedom and j the mode.

A2. Modal participation factors

The participation factors and the effective participation factors are calculated from the inhomogeneous equation of motion. The first step is to construct the nonsingular modeshape matrix F in the following way:

$$F = \{ \underline{f}^1, \underline{f}^2, \ldots, \underline{f}^N \} \qquad (A16)$$

The solution $\underline{Y}$ can then be written as

$$\underline{Y}(t) = F\,\underline{y}(t)$$

where $\underline{y}(t)$ is a vector of time varying coefficients. Substituting

for $\underline{Y}$ in Equation A1 and premultiplying by F^T gives

$$F^T M F \ddot{\underline{y}} + F^T C F \dot{\underline{y}} + F^T K F \underline{y} = - F^T M \ddot{X}\underline{i} \qquad (A17)$$

The effective mass, damping and stiffness matrices are defined by the the following expressions:

$$\begin{aligned} M_e &= F^T M F \\ C_e &= F^T C F \\ K_e &= F^T K F \ . \end{aligned} \qquad (A18)$$

Because of the nature of M and making use of Lagrange's trigonometric identities to solve for the product $F^T F$, M_e can be rewritten as

$$\begin{aligned} M_e &= m F^T F \\ &= 1/4 \ (2N+1) \ m \ I \ . \end{aligned} \qquad (A19)$$

Premultiplying Equation A17 by M_e^{-1} leads to

$$\ddot{\underline{y}} + M_e^{-1} C_e \dot{\underline{y}} + M_e^{-1} K_e \underline{y} = - \ddot{X} \underline{p} \qquad (A20)$$

where the vector $\underline{p}$ contains the participation factors. The vector $\underline{p}$ is given by

$$\begin{aligned} \underline{p} &= M_e^{-1} F^T M \underline{i} \\ &= \frac{4}{(2N+1)} F^T \underline{i} \end{aligned} \qquad (A21)$$

which, in components, takes the form

$$p_j = \frac{1}{N+1/2} \frac{\cos \pi[(2j-1)/(4N+2)] - \cos \pi[(2j-1)/2]}{\sin \pi[(2j-1)/(4N+2)]} . \qquad (A22)$$

The effective participation factors are defined as

$$p_i^{(j)} = F_{ij}\, p_j \qquad (A23)$$

where the index i refers to the degree-of-freedom and j refers to the mode. For a ten degree-of-freedom shear building, the effective participation factors associated with the tenth degree-of-freedom (N=10) are given by

$$p_{10}^{(j)} = \frac{1}{10.5} \sin \pi \left(10 \frac{2j-1}{21}\right) \frac{\cos \pi [(2j-1)/42] - \cos \pi [(2j-1)/2]}{\sin \pi [(2j-1)/42]}. \qquad (A24)$$

Values of these factors for the ten modes are given in Table 2 in the report.

A3. Appendix A - References

1. T. K. Caughey and M. E. J. O'Kelly, "Classical Normal Modes in Damped Linear Dynamic Systems", J. Appl. Mech., ASME, 32, pp. 583-588. 1965.

CALIFORNIA INSTITUTE OF TECHNOLOGY

Reports Published

by

Earthquake Engineering Research Laboratory*
Dynamic Laboratory
Disaster Research Center

Note: Numbers in parenthesis are Accession Numbers assigned by the National Technical Information Service; these reports may be ordered from the National Technical Information Service, 5285 Port Royal Road, Springfield, Virginia, 22161. Accession Numbers should be quoted on orders for reports (PB --- ---). Reports without this information either have not been submitted to NTIS or the information was not available at the time of printing. An N/A in parenthesis indicates that the report is no longer available at Caltech.

1. Alford, J.L., G.W. Housner and R.R. Martel, "Spectrum Analysis of Strong-Motion Earthquake," 1951. (Revised August 1964). (N/A)

2. Housner, G.W., "Intensity of Ground Motion During Strong Earthquakes," 1952. (N/A)

3. Hudson, D.E., J.L. Alford and G.W. Housner, "Response of a Structure to an Explosive Generated Ground Shock," 1952. (N/A)

4. Housner, G.W., "Analysis of the Taft Accelerogram of the Earthquake of 21 July 1952." (N/A)

5. Housner, G.W., "A Dislocation Theory of Earthquakes," 1953. (N/A)

6. Caughey, T.K., and D.E. Hudson, "An Electric Analog Type Response Spectrum," 1954. (N/A)

7. Hudson, D.E., and G.W. Housner, "Vibration Tests of a Steel-Frame Building," 1954. (N/A)

8. Housner, G.W., "Earthquake Pressures on Fluid Containers," 1954. (N/A)

9. Hudson, D.E., "The Wilmot Survey Type Strong-Motion Earthquake Recorder," 1958. (N/A)

10. Hudson, D.E., and W.D. Iwan, "The Wilmot Survey Type Strong-Motion Earthquake Recorder, Part II," 1960. (N/A)

* To order directly by phone the number is 703-487-4650.

11. Caughey, T.K., D.E. Hudson, and R.V. Powell, "The CIT Mark II Electric Analog Type Response Spectrum Analyzer for Earthquake Excitation Studies," 1960. (N/A)

12. Keightley, W.O., G.W. Housner and D.E. Hudson, "Vibration Tests of the Encino Dam Intake Tower," 1961. (N/A)

13. Merchant, Howard Carl, "Mode Superposition Methods Applied to Linear Mechanical Systems Under Earthquake Type Excitation," 1961. (N/A)

14. Iwan, Wilfred D., "The Dynamic Response of Bilinear Hysteretic Systems," 1961. (N/A)

15. Hudson, D.E., "A New Vibration Exciter for Dynamic Test of Full-Scale Structures," 1961. (N/A)

16. Hudson, D.E., "Synchronized Vibration Generators for Dynamic Tests of Full-Scale Structures," 1962. (N/A)

17. Jennings, Paul C., "Velocity Spectra of the Mexican Earthquakes of 11 May and 19 May 1962," 1962. (N/A)

18. Jennings, Paul C., "Response of Simple Yielding Structures to Earthquake Excitation," 1963. (N/A)

19. Keightley, Willard O., "Vibration Tests of Structures," 1963. (N/A)

20. Caughey, T.K., and M.E.J. O'Kelly, "General Theory of Vibration of Damped Linear Dynamic Systems," 1963. (N/A)

21. O'Kelly, M.E.J., "Vibration of Viscously Damped Linear Dynamic Systems," 1964. (N/A)

22. Nielsen, N. Norby, "Dynamic Response of Miltistory Buildings," 1964. (N/A)

23. Tso, Wai Keung, "Dynamics of Thin-Walled Beams of Open Section," 1964. (N/A)

24. Keightley, Willard O., "A Dynamic Investigation of Bouquet Canyon Dam," 1964. (N/A)

25. Malhotra, R.K., "Free and Forced Oscillations of a Class of Self-Excited Oscillators," 1964.

26. Hanson, Robert D., "Post-Elastic Response of Mild Steel Structures," 1965.

27. Masri, Sami F., "Analytical and Experimental Studies of Impact Dampers," 1965.

28. Hanson, Robert D., "Static and Dynamic Tests of a Full-Scale Steel-Frame Structures," 1965.

29. Cronin, Donald L., "Response of Linear, Viscous Damped Systems to Excitations Having Time-Varying Frequecy," 1965.

30. Hu, Paul Yu-fei, "Analytical and Experimental Studies of Random Vibration," 1965.

31. Crede, Charles E., "Research on Failure of Equipment when Subject to Vibration," 1965.

32. Lutes, Loren D., "Numerical Response Characteristics of a Uniform Beam Carrying One Discrete Load," 1965. (N/A)

33. Rocke, Richard D., "Transmission Matrices and Lumped Parameter Models for Continuous Systems," 1966. (N/A)

34. Brady, Arthur Gerald, "Studies of Response to Earthquake Ground Motion," 1966. (N/A)

35. Atkinson, John D., "Spectral Density of First Order Piecewise Linear Systems Excited by White Noise," 1967. (N/A)

36. Dickerson, John R., "Stability of Parametrically Excited Differential Equations," 1967. (N/A)

37. Giberson, Melbourne F., "The Response of Nonlinear Multi-Story Structures Subjected to Earthquake Excitation," 1967. (N/A)

38. Hallanger, Lawrence W., "The Dynamic Stability of an Unbalanced Mass Exciter," 1967.

39. Husid, Raul, "Gravity Effects on the Earthquake Response of Yielding Structures," 1967. (N/A)

40. Kuroiwa, Julio H., "Vibration Test of a Multistory Building," 1967. (N/A)

41. Lutes, Loren Daniel, "Stationary Random Response of Bilinear Hysteretic Systems," 1967.

42. Nigam, Navin C., "Inelastic Interactions in the Dynamic Response of Structures," 1967.

43. Nigam, Navin C. and Paul C. Jennings, "Digital Calculation of Response Spectra from Strong-Motion Earthquake Records," 1968.

44. Spencer, Richard A., "The Nonlinear Response of Some Multistory Reinforced and Prestressed Concrete Structures Subjected to Earthquake Excitation," 1968. (N/A)

45. Jennings, P.C., G.W. Housner and N.C. Tsai, "Simulated Earthquake Motions," 1968.

46. "Strong-Motion Instrumental Data on the Borrego Mountain Earthquake of 9 April 1968," (USGS and EERL Joint Report), 1968.

47. Peters, Rex B., "Strong Motion Accelerograph Evaluation," 1969.

48. Heitner, Kenneth L., "A Mathematical Model for Callculation of the Run-Up of Tsunamis," 1969.

49. Trifunac, Mihailo D., "Investigation of Strong Earthquake Ground Motion," 1969. (N/A)

50. Tsai, Nien Chien, "Influence of Local Geology on Earthquake Ground Motion," 1969. (N/A)

51. Trifunac, Mihailo D., "Wind and Microtremor Induced Vibrations of a Twenty-Two Steel Frame Building," EERL 70-01, 1970.

52. Yang, I-Min, "Stationary Random Response of Multidegree-of-Freedom Systems," DYNL-100, June 1970. (N/A)

53. Patula, Edward John, "Equivalent Differential Equations for Nonlinear Dynamic Systems," DYNL-101, June 1970.

54. Prelewicz, Daniel Adam, "Range of Validity of the Method of Averaging," DYNL-102, 1970.

55 Trifunac, M.D., "On the Statistics and Possible Triggering Mechanism of Earthquakes in Southern California," EERL 70-03, July 1970.

56. Heitner, Kenneth Leon, "Additional Investigations on a Mathematical Model for Calculation of Run-Up of Tsunamis," July 1970.

57. Trifunac, Mihailo D., "Ambient Vibration Tests of a Thirty-Nine Story Steel Frame Building," EERL 70-02, July 1970.

58. Trifunac, Mihailo D. and D.E. Hudson, "Laboratory Evaluations and Instrument Corrections of Strong-Motion Accelerographs," EERL 70-04, August 1970. (N/A)

59. Trifunac, Mihailo D., "Response Envelope Spectrum and Interpretation of Strong Earthquake Groun Motion," EERL 70-06, August 1970.

60. Keightley, W.O., "A Strong-Motion Accelerograph Array with Telephone Line Interconnections," EERL 70-05, September 1970.

61. Trifunac, Mihailo D., "Low Frequency Digitization Errors and a New Method for Zero Baseline Correction of Strong-Motion Accelerograms," EERL 70-07, September 1970.

62. Vijayaraghavan, A., "Free and Forced Oscillations in a Class of Piecewise-Linear Dynamic Systems," DYNL-103, January 1971.

63. Jennings, Paul C., R.B. Mathiesen and J. Brent Hoerner, "Forced Vibrations of a 22-Story Steel Frame Building," EERL 71-01, February 1971. (N/A) (PB 205 161)

64. Jennings, Paul C., "Engineering Features of the San Fernando Earthquake of February 9, 1971," EERL 71-02, June 1971. (PB 202 550)

65. Bielak, Jacobo, "Earthquake Response of Building-Foundation Systems," EERL 71-04, June 1971. (N/A) (PB 205 305)

66. Adu, Randolph Ademola, "Response and Failure of Structures Under Stationary Random Excitation," EERL 71-03, June 1971. (N/A) (PB 205 304)

67. Skattum, Knut Sverre, "Dynamic Analysis of Coupled Shear Walls and Sandwich Beams," EERL 71-06, June 1971. (N/A) (PB 205 267)

68. Hoerner, John Brent, "Model Coupling and Earthquake Response of Tall Buildings," EERL 71-07, June 1971. (N/A) (PB 207 635)

69. Stahl, Karl John, "Dynamic Response of Circular Plates Subjected to Moving Massive Loads," DYNL-104, June 1971. (N/A)

70. Trifunac, M.D., F.E. Udwadia and A.G. Brady, "High Frequency Errors and Instrument Corrections of Strong-Motion Accelerograms," EERL 71-05, 1971. (PB 205 369)

71. Furuike, D.M., "Dynamic Response of Hysteretic Systems With Application to a System Containing Limited Slip," DYNL-105, September 1971. (N/A)

72. Hudson, D.E. (Editor), "Strong-Motion Instrumental Data on the San Fernando Earthquake of February 9, 1971," (Seismological Field Survey, NOAA, C.I.T. Joint Report), September 1971. (PB 204 198)

73. Jennings, Paul C. and Jacobo Bielak, "Dynamics of Building-Soil Interaction," EERL 72-01, April 1972. (PB 209 666)

74. Kim, Byung-Koo, "Piesewise Linear Dynamic Systems with Time Delays," DYNL-106, April 1972.

75. Viano, David Charles, "Wave Propagation in a Symmetrically Layered Elastic Plate," DYNL-107, May 1972.

76. Whitney, Albert W., "On Insurance Settlements Incident to the 1906 San Francisco Fire," DRC 72-01, August 1972. (PB 213 256)

77. Udwadia, F.E., "Investigation of Earthquake and Microtremor Ground Motions," EERL 72-02, September 1972. (PB 212 853)

78. Wood, John H., "Analysis of the Earthquake Response of a Nine-Story Steel Frame Building During the San Fernando Earthquake," EERL 72-04, October 1972. (PB 215 823)

79. Jennings, Paul C., "Rapid Calculation of Selected Fourier Spectrum Ordinates," EERL 72-05, November 1972.

80. "Research Papers Submitted to Fifth World Conference on Earthquake Engineering, Rome, Italy, 25-29 June 1973," EERL 73-02, March 1973. (PB 220 431)

81. Udwadia, F.E., and M.D. Trifunac, "The Fourier Transform, Response Spectra and Their Relationship Through the Statistics of Oscillator Response," EERL 73-01, April 1973. (PB 220 458)

82. Housner, George W., "Earthquake-Resistant Design of High-Rise Buildings," DRC 73-01, July 1973. (N/A)

83. "Earthquake and Insurance," Earthquake Research Affiliates Conference, 2-3 April, 1973, DRC 73-02, July 1973. (PB 223 033)

84. Wood, John H., "Earthquake-Induced Soil Pressures on Structures," EERL 73-05, August 1973. (N/A)

85. Crouse, Charles B., "Engineering Studies of the San Fernando Earthquake," EERL 73-04, March 1973. (N/A)

86. Irvine, H.Max, "The Veracruz Earthquake of 28 August 1973," EERL 73-06, October 1973.

87. Iemura, H. and P.C. Jennings, "Hysteretic Response of a Nine-Story Reinforced Concrete Building During the San Fernando Earthquake," EERL 73-07, October 1973.

88. Trifunac, M.D. and V. Lee, "Routine Computer Processing of Strong-Motion Accelerograms," EERL 73-03, October 1973. (N/A) (PB 226 047/AS)

89. Moeller, Thomas Lee, "The Dynamics of a Spinning Elastic Disk with Massive Load," DYNL 73-01, October 1973.

90. Blevins, Robert D., "Flow Induced Vibration of Bluff Structures," DYNL 74-01, February 1974.

91. Irvine, H. Max, "Studies in the Statics and Dynamics of Simple Cable Systems," DYNL-108, January 1974.

92. Jephcott, D.K. and D.E. Hudson, "The Performance of Public School Plants During the San Fernando Earthquake," EERL 74-01, September 1974. (PB 240 000/AS)

93. Wong, Hung Leung, "Dynamic Soil-Structure Interaction," EERL 75-01, May 1975. (N/A) (PB 247 233/AS)

94. Foutch, D.A., G.W. Housner, and P.C. Jennings, "Dynamic Responses of Six Multistory Buildings During the San Fernando Earthquake," EERL 75-02, October 1975. (PB 248 144/AS)

95. Miller, Richard Keith, "The Steady-State Response of Multidegree-of-Freedom Systems with a Spatially Localized Nonlinearity," EERL 75-03, October 1975. (PB 252 459/AS)

96. Abdel-Ghaffar, Ahmed Mansour, "Dynamic Analyses of Suspension Bridge Structures," EERL 76-01, May 1976. (PB 258 744/AS)

97. Foutch, Douglas A., "A Study of the Vibrational Characteristics of Two Multistory Buildings," EERL 76-03, September 1976. (PB 260 874/AS)

98. "Strong Motion Earthquake Accelerograms Index Volume," Earthquake Engineering Research Laboratory, EERL 76-02, August 1976. (PB 260 929/AS)

99. Spanos, P-T.D., "Linearization Techniques for Non-Linear Dynamical Systems," EERL 76-04, September 1976. (PB 266 083/AS)

100. Edwards, Dean Barton, "Time Domain Analysis of Switching Regulators," DYNL 77-01, March 1977.

101. Abdel-Ghaffar, Ahmed Mansour, "Studies of the Effect of Differential Motions of Two Foundations upon the Response of the Superstructure of a Bridge," EERL 77-02, January 1977. (PB 271 095/AS)

102. Gates, Nathan C., "The Earthquake Response of Deteriorating Systems," EERL 77-03, March 1977. (PB 271 090/AS)

103. Daly, W., W. Judd and R. Meade, "Evaluation of Seismicity at U.S. Reservoirs," USCOLD, Committee on Earthquakes, May 1977. (PB 270 036/AS)

104. Abdel-Ghaffer, A.M. and G.W. Housner, "An Analysis of the Dynamic Characteristics of a Suspension Bridge by Ambient Vibration Measurements," EERL 77-01, January 1977. (PB 275 063/AS)

105. Housner, G.W. and P.C. Jennings, "Earthquake Design Criteria for Structures," EERL 77-06, November 1977. (PB 276 502/AS)

106. Morrison, P., R. Maley, G. Brady, R. Porcella, "Earthquake Recordings on or Near Dams," USCOLD, Committee on Earthquakes, November 1977. (PB 285 867/AS)

107. Abdel-Ghaffar, A.M., "Engineering Data and Analyses of the Whittier, California Earthquake of January 1, 1976," EERL 77-05, November 1977. (PB 283 750/AS)

108. Beck, James L., "Determining Models of Structures from Earthquake Records," EERL 78-01, June 1978. (PB 288 806/AS)

109. Psycharis, Ioannis, "The Salonica(Thessaloniki) Earthquake of June 20, 1978," EERL 78-03, October 1978. (PB 290 120/AS)

110. Abdel-Ghaffar, A.M. and R.F. Scott, "An Investigation of the Dynamic Characteristics of an Earth Dam," EERL 78-02, August 1978. (PB 288 878/AS)

111. Mason, Alfred B., Jr., "Some Observations on the Random Response of Linear and Nonlinear Dynamical Systems," EERL 79-01, January 1979. (PB 290 808/AS)

112. Helmberger, D.V. and P.C. Jennings (Organizers), "Strong Ground Motion: N.S.F. Seminar-Workshop," SL-EERL 79-02, February 1978.

113. Lee, David M., Paul C. Jennings and George W. Housner, "A Selection of Important Strong Motion Earthquake Records," EERL 80-01, January 1980. (PB 80 169196)

114. McVerry, Graeme H., "Frequency Domain Identification of Structural Models from Earthquake Records," EERL 79-02, October 1979. (PB-80-194301)

115. Abdel-Ghaffar A.M., R.F.Scott and M.J.Craig, "Full-Scall Experimental Investigation of a Modern Earth Dam," EERL 80-02, February 1980. (PB-81-123788)

116. Rutenberg, Avigdor, Paul C. Jennings and George W. Housner, "The Response of Veterans Hospital Building 41 in the San Fernando Earthquake," EERL 80-03, May 1980. (PB-82-201377)

117. Haroun, Medhat Ahmed, "Dynamic Analyses of Liquid Storage Tanks," EERL 80-04, February 1980. (PB-81-123275)

118. Liu, Wing Kam, "Development of Finite Element Procedures for Fluid-Structure Interaction," EERL 80-06, August 1980. (PB 184078)

119. Yoder, Paul Jerome, "A Strain-Space Plasticity Theory and Numerical Implementation," EERL 80-07, August 1980. (PB-82-201682)

120. Krousgrill, Charles Morton, Jr., "A Linearization Technique for the Dynamic Response of Nonlinear Continua," EERL 80-08, September 1980. (PB-82-201823)

121. Cohen, Martin, "Silent Boundary Methods for Transient Wave Analysis," EERL 80-09, September 1980. (PB-82-201831)

122. Hall, Shawn A., "Vortex-Induced Vibrations of Structures," EERL 81-01, January 1981. (PB-82-201849)

123. Psycharis, Ioannis N., "Dynamic Behavior of Rocking Structures Allowed to Uplift," EERL 81-02, August 1981. (PB-82-212945)

124. Shih, Choon-Foo, "Failure of Liquid Storage Tanks Due to Earthquake Excitation," EERL 81-04, May 1981. (PB-82-215013)

125. Lin, Albert Niu, "Experimental Observations of the Effect of Foundation Embedment on Structural Response," EERL 82-01, May 1982. (PB-84-163252)

126. Botelho, Dirceau L.R., "An Empirical Model for Vortex-Induced Vibrations," EERL 82-02, August 1982. (PB-84-161157)

127. Ortiz, L. Alexander, "Dynamic Centrifuge Testing of Cantilever Retaining Walls," SML 82-02, August 1982. (PB-84-162312)

128. Iwan, W.D., Editor, "Proceedings of the U.S. National Workshop on Strong-Motion Earthquake Instrumentation, April 12-14, 1981, Santa Barbara, California," California Institute of Technology, Pasadena, California, 1981.

129. Rashed, Ahmed, "Dynamic Analysis of Fluid-Structure Systems," EERL 82-03, July 1982. (PB-84-162916)

130. National Academy Press, "Earthquake Engineering Research-1982."

131. National Academy Press, "Earthquake Engineering Research-1982, Overview and Recommendations."

132. Jain, Sudhir Kumar, "Analytical Models for the Dynamics of Buildings," EERL 83-02, May 1983. (PB-84-161009)

133. Huang, Moh-Jiann, "Investigation of Local Geology Effects on Strong Earthquake Ground Motions," EERL 83-03, July 1983. PB-

134. Mcverry, G.H. and J.L. Beck, "Structural Identification of JPL Building 180 Using Optimally Synchronized Earthquake Records." EERL 83-01, August 1983. PB-

135. Bardet, J.P., "Application of Plasticity Theory to Soil Behavior: A New Sand Model," SML 83-01, September 1983. (PB-84-162304)

136. Wilson, John C., "Analysis of the Observed Earthquake Response of a Multiple Span Bridge," EERL 84-01, May 1984. PB-

137. Hushmand, Behnam, "Experimental Studies of Dynamic Response of Foundations," SML 83-02, November 1983. PB-

138. Cifuentes, Arturo O., "System Identification of Hysteretic Structures," EERL 84-04, 1984. PB-

139. Smith, Kenneth Scott, "Stochastic Analysis of the Seismic Response of Secondary Systems," EERL 85-01, November 1984. PB-

140. Maragakis, Emmanuel, "A Model for the Rigid Body Motions of Skew Bridges," EERL 85-02, December 1984. PB-

141. Jeong, Garrett Duane, "Cumulative Damage of Structures Subjected to Response Spectrum Consistent Random Process," EERL 85-03, January 1985. PB-

Strong-Motion Earthquake Accelerograms
Digitized and Plotted Data

Uncorrected Accelerograms

Volume I

Part	Report No.	NTIS Accession No.
A	EERL 70-20	PB 287 847
B	EERL 70-21	PB 196 823
C	EERL 71-20	PB 204 364
D	EERL 71-21	PB 208 529
E	EERL 71-22	PB 209 749
F	EERL 71-23	PB 210 619
G	EERL 72-20	PB 211 357
H	EERL 72-21	PB 211 781
I	EERL 72-22	PB 213 422
J	EERL 72-23	PB 213 423
K	EERL 72-24	PB 213 424
L	EERL 72-25	PB 215 639
M	EERL 72-26	PB 220 554
N	EERL 72-27	PB 223 023
O	EERL 73-20	PB 222 417
P	EERL 73-21	PB 227 481/AS
Q	EERL 73-22	PB 232 315/AS
R	EERL 73-23	PB 239 585/AS
S	EERL 73-24	PB 241 551/AS
T	EERL 73-25	PB 241 943/AS
U	EERL 73-26	PB 242 262/AS
V	EERL 73-27	PB 243 483/AS
W	EERL 73-28	PB 243 497/AS
X	EERL 73-29	PB 243 594/AS
Y	EERL 73-30	PB 242 947/AS

Strong-Motion Earthquake Accelerograms
Digitized and Plotted Data

Corrected Accelerograms and Integrated
Ground Velocity and Displacement Curves

Volume II

Part	Report No.	NTIS Accession No.
A	EERL 71-50	PB 208 283
B	EERL 72-50	PB 220 161
C	EERL 72-51	PB 220 162
D	EERL 72-52	PB 220 836
E	EERL 73-50	PB 223 024
F	EERL 73-51	PB 224 977/9AS
G	EERL 73-52	PB 229 239/AS
H	EERL 74-50	PB 231 225/AS
I	EERL 74-51	PB 232 316/AS
J,K	EERL 74-52	PB 233 257/AS
L,M	EERL 74-53	PB 237 174/AS
N	EERL 74-54	PB 236 399/AS
O,P	EERL 74-55	PB 239 586/AS
Q,R	EERL 74-56	PB 239 587/AS
S	EERL 74-57	PB 241 552/AS
T	EERL 75-50	PB 242 433/AS
U	EERL 75-51	PB 242 949/AS
V	EERL 75-52	PB 242 948/AS
W,Y	EERL 75-53	PB 243 719

Analyses of Strong-Motion Earthquake Accelerograms
Response Spectra

Volume III

Part	Report No.	NTIS Accession No.
A	EERL 72-80	PB 212 602
B	EERL 73-80	PB 221 256
C	EERL 73-81	PB 223 025
D	EERL 73-82	PB 227 469/AS
E	EERL 73-83	PB 227 470/AS
F	EERL 73-84	PB 227 471/AS
G	EERL 73-85	PB 231 223/AS
H	EERL 74-80	PB 231 319/AS
I	EERL 74-81	PB 232 326/AS
J,K,L	EERL 74-82	PB 236 110/AS
M,N	EERL 74-83	PB 236 400/AS
O,P	EERL 74-84	PB 238 102/AS
Q,R	EERL 74-85	PB 240 688/AS
S	EERL 74-86	PB 241 553/AS
T	EERL 75-80	PB 243 698/AS
U	EERL 75-81	PB 242 950/AS
V	EERL 75-82	PB 242 951/AS
W,Y	EERL 75-83	PB 243 492/AS

Analyses of Strong-Motion Earthquake Accelerograms
Fourier Amplitude Spectra

Volume IV

Part	Report No.	NTIS Accession No.
A	EERL 72-100	PB 212 603
B	EERL 73-100	PB 220 837
C	EERL 73-101	PB 222 514
D	EERL 73-102	PB 222 969/AS
E	EERL 73-103	PB 229 240/AS
F	EERL 73-104	PB 229 241/AS
G	EERL 73-105	PB 231 224/AS
H	EERL 74-100	PB 232 327/AS
I	EERL 74-101	PB 232 328/AS
J,K,L,M	EERL 74-102	PB 236 111/AS
N,O,P	EERL 74-103	PB 238 447/AS
Q,R,S	EERL 74-104	PB 241 554/AS
T,U	EERL 75-100	PB 243 493/AS
V,W,Y	EERL 75-101	PB 243 494/AS
Index Volume	EERL 76-02	PB 260 929/AS